Use of Machine Learning in Micro-plasma Metal Additive Manufacturing Process for Optimum Deposition Geometry

M.Tech. Thesis

By

Anubhav Vaishnav

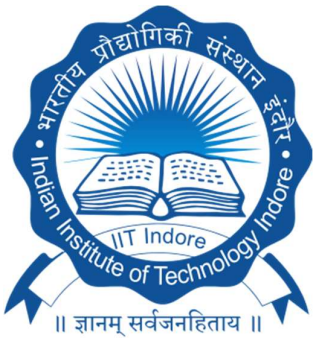

Department of Mechanical Engineering

Indian Institute of Technology Indore

June 2025

Use of Machine Learning in Micro-plasma Metal Additive Manufacturing Process for Optimum Geometry of Deposition

A THESIS

Submitted in partial fulfilment of
the requirements for the award of
the degree

of

Master of Technology

by

Anubhav Vaishnav

Department of Mechanical Engineering

Indian Institute of Technology Indore

June 2025

Indian Institute of Technology Indore

Candidate's Declaration

I hereby certify that the work which is being presented in the thesis entitled "**Use of Machine Learning in Micro-plasma Metal Additive Manufacturing Process for Optimum Geometry of Deposition**" in the partial fulfillment of the requirements for the award of the degree of **Master of Technology** and submitted to the **Department of Mechanical Engineering, Indian Institute of Technology Indore**, is an authentic record of my own work carried out during the time period from **July 2023** to **May 2025** under the supervision of **Prof. Neelesh Kumar Jain**, Professor (HAG), IIT Indore and **Dr. Sagar H. Nikam**, Lecturer, School of Computing, Engineering, and Intelligent Systems, Ulster University, Derry/Londonderry (UK). The matter presented in this thesis has not been submitted by me for the award of any other degree of this or any other institute.

10th June 2025
Anubhav Vaishnav

This is to certify that the above statement made by the candidate is correct to the best of our knowledge.

16th June 2025
Signature of 1st Supervisor of M.Tech. thesis (with date)
(Prof. Neelesh Kumar Jain)

16th June 2025
Signature of 2nd Supervisor of M.Tech. thesis (with date)
(Dr. Sagar H. Nikam)

Anubhav Vaishnav has successfully given his M.Tech. Oral Examination held on **26th May 2025.**

Signatures of M.Tech. Thesis Supervisors
Date: **16th June 2025**

Signature of DPGC Convener
Date: 17/06/25

Abstract

Micro-plasma metal additive manufacturing (μ-PMAM) is a highly precise and energy-efficient process to fabricate the metallic components. But, achieving consistent deposition geometry remains challenging due to the complex interactions among process parameters and dynamics of different deposition layers. This thesis presents noble approach of employing machine learning (ML) and deep learning (DL) respectively to predict and optimize geometry of single-layer and multi-layer depositions fabricated by the μ-PMAM process. A high dynamic range (HDR) camera was used to record videos of single-layer depositions of Ti6Al4V on the same material base plate and single-layer and multi-layer depositions of SS 316L on a mild streel base plate for different combinations of μ-PMAM process parameters (such as μ-plasma power, feedstock powder flow rate, worktable feed rate for single-layer deposition and additional parameters namely stand-off-distance, deposition layer index, height and width of previously deposited layer, and cumulative height for multi-layer depositions). Images were extracted from each recorded video at a rate of 30 frames per second. The extracted images were annotated and feature scaling was performed for the single-layer depositions and the Histogram based Multi-Mode method was used for multi-layer depositions to generate the datasets. The generated datasets were split into training, validation, and test data to ensure robust model development. Six ML algorithms and three DL algorithms were trained using the generated datasets for single-layer and multi-layer depositions respectively. The trained algorithms were evaluated using the performance matrix involving mean absolute error, root-mean-square error, and coefficient of determination to select the top performing ML and DL algorithm. It selected the Random Forest (RF) algorithm for predicting height and width of single-layer depositions, and Self-Attention Temporal Convolutional Network (SA-TCN) for multi-layer depositions. The selected ML and DL models were trained, tested and validated. Then they were integrated with Non-dominated Sorting Genetic Algorithm II (NSGA-II) to perform multi-objective optimization using objective functions as the difference between the desired and ML/DL algorithm predicted values for deposition height, deposition width, and aspect ratio. The optimized results demonstrate that this integrated approach reduced geometric prediction errors below 5% thus offering a systematic alternative to trial-and-error tuning of μ-PMAM process parameters. The methodology of the present work provides a scalable solution for closed-loop control for any AM process and lays the foundation for development of its digital twin. It also highlights the transformative potential of artificial intelligence in advancing metal additive manufacturing processes.

List of Publications

1. **Anubhav Vaishnav**, Neelesh Kumar Jain, Sagar Nikam, Deepika Nikam, Balbir Singh Negi, Pradyumn Kumar Arya, "*Machine learning based geometry predictions for single and multi-layer depositions by μ-PMAM process and its multi-objective optimization*" submitted to the ***Machine Learning*** (**Impact factor: 4.3**)

2. **Anubhav Vaishnav**, Kartik Chaudhary, Neelesh Kumar Jain, Sagar Nikam, Deepika Nikam, Balbir Singh Negi, Pradyumn Kumar Arya "*Integrating computer vision and machine learning for real-time detection and elimination of deposition defects in μ-plasma metal additive manufacturing process*" submitted to the ***Journal of Intelligent Manufacturing*** (**Impact factor: 5.9**)

Acknowledgements

I take this opportunity to express my deep sense of respect and gratitude towards my thesis supervisors Prof. Neelesh Kumar Jain and Dr. Sagar Nikam for believing in me to carry out this work under their supervision. Their constant encouragement and constructive support have enabled this work to achieve its present form. Their innovative perspective towards things and their continuous pursuit for perfection has had a profound effect on me and has transformed me majorly. I feel great privileged to be one of their students. I am also thankful to all the faculties of our Mechanical Engineering Department for supporting and providing us facilities, their moral support, and friendly environment throughout my M. Tech program.

I express my deep sense of gratitude to PhD scholars Balbir Singh Negi, Pradyumn Kumar Arya, Rahul Naidu and Ravindra Verma for bearing with me and for supporting me morally and technically and always maintaining a homely atmosphere in the lab. It would be incomplete to end these acknowledgments without conveying my heartfelt gratitude and deep reverence to my beloved parents and close friends for their unwavering blessings and moral support throughout the journey of this work.

Anubhav Vaishnav

Dedicated

to

My parents and Sister

Table of Contents

Contents	Page No.
List of Figures ……	xix
List of Tables ……	xxi
Acronyms ……...	xxiii
Chapter 1: Introduction ……..	1-20
1.1 Machine Learning (ML) …….	1
1.1.1 Types of Learning for ML Algorithms …….	1
1.1.2 Types of ML Algorithms ……..	4
1.1.3 Applications of ML in Manufacturing …….	5
1.1.4 Applications of ML in Additive Manufacturing ……..	6
1.2 Deep Learning (DL) ……...	7
1.2.1 Types of Deep Learning Algorithms ……	7
1.2.2 Applications of DL in Manufacturing ……..	8
1.2.3 Applications of DL in Additive Manufacturing ……...	9
1.3 Additive Manufacturing ……..	9
1.3.1 Classification of AM Processes ……	10
1.3.2 Advantages of AM Processes ……...	12
1.3.3 Limitations of AM Processes ……...	13
1.3.4 Applications of AM Processes …….	14
1.4 Directed Energy Deposition (DED) Processes ……...	15
1.4.1 Types of DED Processes ……..	15
1.4.2 Advantages of DED Processes …….	16
1.4.3 Limitations of DED Processes …….	17
1.4.4 Applications of DED Processes ……...	17
1.5 Micro-Plasma Metal Additive Manufacturing (μ-PMAM) ……	17
1.5.1 Applications of μ-PMAM Process ……...	19
1.6 Organization of the Thesis ……..	19

Chapter 2: Review of the Past Work ……	21-27
2.1 Past Work on ML Usage in AM Processes …….	21
2.1.1 Detection and Minimization of Deposition Defects Using ML/DL …….	21
2.1.2 Deposition Geometry Optimization Using ML/DL …….	22
2.1.3 Summary of Past Work Review ……	24
2.2 Identified Research Gaps ……	25
2.3 Research Objectives ……	25
2.4 Research Methodology ……...	25
Chapter 3: Materials and Methods ……	29-45
3.1 Selection of Deposition and Base Plate Materials ……..	29
3.2 Selection of Input Parameters …….	30
3.3 Data Acquisition …….	31
3.4 Processing of the Recoded Videos …….	32
3.4.1 Extraction of Images from the Recorded Videos …….	33
3.4.2 Feature Scaling of Single-Layer Depositions Data ……..	33
3.4.3 Histogram-Based Multi-Modal Method for Multi-Layer Depositions …	35
3.4.4 Splitting of Datasets …….	37
3.5 Selection and Training of ML Algorithms for Single-Layer Depositions ……...	38
3.6 Selection and Training of DL Algorithms for Multi-Layer Deposition …….	39
3.7 Evaluation of the Trained ML and DL Algorithms ……	39
3.8 Selection of Appropriate ML and DL Algorithm ……...	41
3.9 Training of the Selected ML and DL Algorithm …….....	42
3.9.1 Random Forest Algorithm for Single-Layer Depositions ……	42
3.9.2 SA-TCN Algorithm for Multi-Layer Depositions ……	43
3.10 Multi-Objective Optimization using NSGA-II …….	43

Chapter 4: Results and Discussion ……..	47-53
4.1 Performance of the Selected ML and DL Algorithm …….	47
4.2 Multi-Objective Optimization Results ……	48
4.2.1 Results of NSGA-II ……..	48
4.2.2 Results by NSGA-II Integrated with RF Algorithm for Single-Layer Depositions ……	51
4.2.3 Results of NSGA-II Integrated with SA-TCN Algorithm for Multi-Layer Depositions ……	53
Chapter 5: Conclusions and Scope for Future Work ……	55-57
5.1 Significant Achievements ……...	55
5.2 Conclusions …….	55
5.3 Scope for Future Work ……...	56
References ……	59-60

List of Figures

Details of Figure	Page No.
Fig. 1.1: Relationship between the AI, ML, and DL …….	2
Fig. 1.2: Concept of the supervised learning …….	2
Fig. 1.3: Concept of the unsupervised learning ……..	3
Fig. 1.4: Concept of the reinforcement learning ……	4
Fig. 1.5: Classification of AM processes according to ASTM F42 **(Rafiee et. al. 2020)** .	10
Fig. 1.6: Photograph of the 5-axis CNC machine for μ-PMAM process showing the deposition head and formation of μ-plasma arc inside the μ-plasma torch in the insets …	18
Fig. 2.1: Research mmethodology used in the present work …….	26
Fig. 3.1: Additional inpur parameters for a multi-layer depositon ……	31
Fig. 3.2: Photograph of the CNC machine of μ-PMAM process showing mounting of the high dynamic range (HDR) camera of make TPS XVC-1000-1100 ……..	32
Fig. 3.3: Performance measures for the (a) six ML algorithms; and (b) three DL algorithms, used in the present study …….	41-42
Fig. 4.1: Comparison the RF algorithm predicted single-layer deposition (a) height, and (b) width, with their corresponding experimental values for the validation and testing data ……...	47
Fig. 4.2: Comparison of the SA-TCN algorithm predicted (a) deposition height, and (b) deposition width for each layer of a multi-layer deposition with their corresponding experimental values taken from their testing data …….	48
Fig. 4.3: Pareto fronts for multi-objective optimization by NSGA-II using training data for (a) single-layer depositions, and (b) multi-layer depositions.	49

List of Tables

Details of Table	Page No.
Table 3.1: Deposition and base plate materials used in single-layer and multi-layer depositions by μ-PMAM process.……	29
Table 3.2: Details of recorded videos for single-layer and multi-layer depositions by μ-PMAM process ……..	32
Table: 3.3: Real-time data generated from the recorded video of single-layer deposition of Ti6Al4V by μ-PMAM process and used for training, validation, and testing of the six ML algorithms ……..	34
Table: 3.4: Histogram-based data generated from the recorded videos of multi-layer depositions of SS 316L and used in the training, validation, and testing of three DL algorithms ……..	37
Table: 3.5: Parameters related to the six ML algorithms used in the present study …..	38
Table 4.1: Percentage error between the desired and the RF predicted geometry parameters for *single-layer* depositions using the NSGA-II optimized process parameters ……	50
Table 4.2: Percentage error between the desired geometry parameters and the SA-TCN predicted parameters for *multi-layer* depositions using the NSGA-II optimized process parameter ……..	50
Table 4.3: Optimized process parameters by NSGA-II integrated with the RF algorithm for different combinations of height and width of *single-layer* depositions .	51
Table 4.4: Optimized process parameters by NSGA-II integrated with SA-TCN algorithm for multi-layer deposition of SS 316L ……..	52

ACRONYMS

µ-PMAM	Micro–Plasma Arc Additive Manufacturing
AI	Artificial Intelligence
AM	Additive Manufacturing
ANN	Artificial Neural Network
Bi-LSTM	Bidirectional Long Short-Term Memory
CNN	Convolutional Neural Networks
CumH	Cumulative Height
DED	Directed Energy Deposition
DL	Deep Learning
GPR	Gaussian Process Regression
HDR	High Dynamic Range
KNN	K-Nearest Neighbours
L-DED	Laser-Based DED
LPBF	Laser Powder Bed Fusion
MAE	Mean Absolute Error
ML	Machine Learning
NSGA-II	Non-dominated Sorting Genetic Algorithm II
PAAM	Plasma Arc Additive Manufacturing
PreH/W	Previously Deposited Layer Height/Width
RF	Random Forest
RN	Recurrent Neural Networks
SA-TCN	Self-Attention Temporal Convolutional Network
SOD	Stand-off-Distance
SVR	Support Vector Regression
WAAM	Wire Arc Additive Manufacturing

Chapter 1

Introduction

This chapter introduces the fundamentals of machine learning (ML) and deep learning (DL). It describes the main types of ML and DL algorithms. It highlights applications of ML and DL in manufacturing and additive manufacturing (AM) for the detection of defects, quality control, and parametric optimization. It provides an overview of different types of AM processes, their advantages, limitations, and key industrial applications. It briefly introduces directed energy deposition (DED) processes and μ-Plasma Metal Additive Manufacturing (μ-PMAM) process, summarizing their principles, key benefits, and major applications. It concludes with the thesis organization.

1.1 Machine Learning

Machine learning (ML) is a part of artificial intelligence (AI). It helps computers to find patterns in data and decide or predict things without detailed instructions for every task. The main concept of ML is its capability to adapt when working with new information and get better at spotting patterns in data over a time period. The ML allows machines to take care of work that used to depend on people, making it possible to solve many difficult challenges. In the recent years, growing data and faster computers have made ML as an important and effective tool in every aspect of science, engineering, and social science. The ML algorithms analyze the past data, known as the training data, to detect patterns and relations. Then the ML algorithms undergo a validation phase where a new dataset is used to fine-tune the hyperparameters of an ML algorithm and to avoid its overfitting issues. The final step is to test an ML algorithm using a new dataset that has not been used in its training and validation phases. This step shows whether an ML algorithm works well in real-world scenarios or not. The ML draws its strength from its learning capability from the previous data. This lets it to organize, predict, group, and explain the information. Deep learning (DL) is a subset of ML that uses artificial neural networks (ANN) with multiple layers to process and learn from the data. It is inspired by functioning of the human brain, enabling computers to recognize complex patterns and make decisions. The DL is widely used for tasks such as image and speech recognition, natural language processing, and autonomous systems. Fig.1.1 depicts the relationship between AI, ML, and DL showing that the AI encompasses both the ML and DL with ML being a subset of AI, and DL being a subset of the ML.

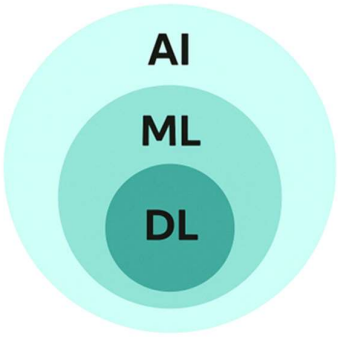

Fig. 1.1: Relationship between the AI, ML, and DL.

1.1.1 Types of Learning for ML Algorithms

The learning process of ML algorithms can be broadly categorized into three major types: supervised learning, unsupervised learning, and reinforcement learning.

- **Supervised Learning:** Supervised learning trains an ML algorithm using the labeled datasets where each data point has a known output. The goal is to make learn an ML algorithm to match input features with the right labels by reducing the difference between the predicted and actual values as shown in Fig. 1.2. It demonstrates how a supervised learning algorithm learns to classify input features, such as shapes, by matching them with their correct labels during training. After the training, an ML algorithm is validated to fine-tune its hyperparameters using a new dataset and to avoid its overfitting issues. Then the algorithm is tested using on a separate dataset to see how well it works in real-world scenarios. Getting the algorithm to handle new data well is the main focus here. Training, validation, and testing together make it possible to build reliable ML algorithms. Supervised learning is used in the fields such as image recognition, improving processes, and predicting maintenance needs. It breaks down into two tasks: regression predicts continuous results such as numbers, while classification assigns things into categories or labels.

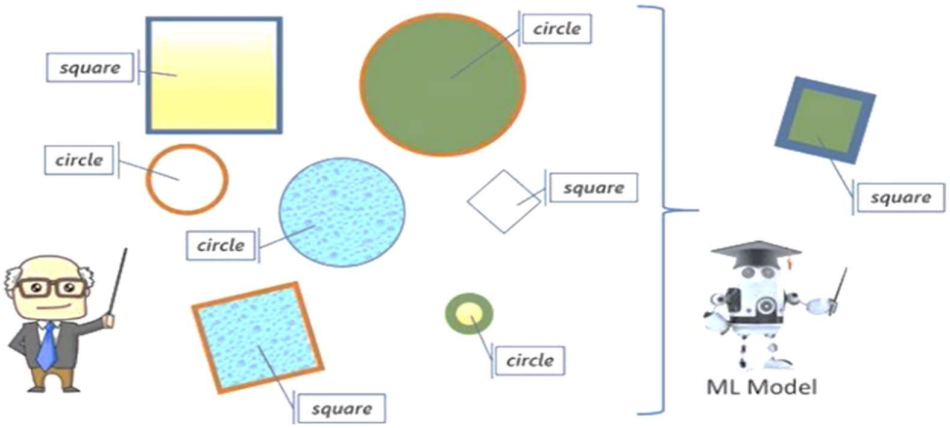

Fig. 1.2: Concept of the supervised learning.

- **Unsupervised Learning:** Unsupervised learning trains an ML algorithm by examining unlabelled data and ignoring the predefined outputs. It does not rely on the correct answers during the training which is the main difference from the supervised learning. It focuses on uncovering hidden structures or trends in raw datasets. It aims to analyse data to simplify understanding or group similar items. Fig. 1.3 illustrates concept of the unsupervised learning process where an AM algorithm analyzes raw, unlabeled data and organizes them into groups based on patterns and similarities without predefined labels. Tools such as principal component analysis (PCA) shrink the large datasets to make their handling simpler. Whereas, techniques such as K-means and hierarchical clustering organize the data into clusters based on their similarities (**Abdulhafedh, 2021**). This learning becomes helpful when labelled data are unavailable or difficult to obtain. In the manufacturing field, unsupervised learning finds patterns in sensor readings, spots strange behaviour, or links equipment with shared conditions. It provides new insights that older methods might overlook and helps make smarter decisions based on data.

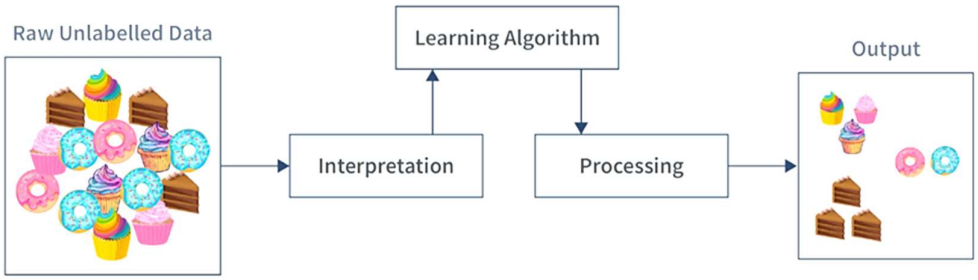

Fig. 1.3: Concept of the unsupervised learning.

- **Reinforcement Learning:** Training of an ML algorithm in the reinforcement learning happens through constant interactions between an autonomous agent and the environment. An autonomous agent is a system that can make decisions and act in response to its environment and which is independent of direct instruction by a human user. The agent performs actions based on the current state, receives feedback as rewards or penalties, and relies on this feedback to make better choices in the future as illustrates in Fig. 1.4. Initially, the agent might have little knowledge and try different actions but it learns from the reward signals which will lead to better results. This cycle continues until performance of the agent reaches a stable point with an aim to develop a policy that earns the highest possible reward over the time. The testing of an ML algorithm requires putting the learned policy into a fresh or unfamiliar environments to see how well the agent adapts. The validation in the reinforcement learning is different from the supervised learning because ability of the autonomous agent is evaluated to check how well it has learned to make decisions tested in a similar environment (**Pitis et al., 2021**).

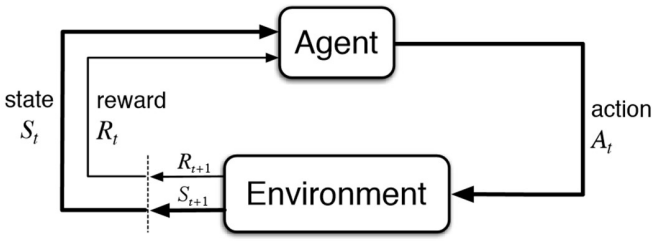

Fig. 1.4: Concept of the reinforcement learning.

Besides the above-mentioned learning methods, following are some mixed learning approaches for the ML algorithms: (i) **Semi-supervised learning**: trains the ML algorithms by using a mix of some labeled data and lot of more unlabeled data, (ii) **Self-supervised learning** uses patterns in the data itself as a guide to train the ML algorithms. For example, algorithms such as Random Forest and Gradient Boosting Machines blend several algorithms together to improve performance and make their predictions more reliable.

1.1.2 Types of ML Algorithms

Following are the commonly used ML algorithms:

- **Random Forest (RF):** It is an ensemble ML algorithm that operates by constructing multiple decision trees during its training and generate either mode of the classes (for the classification purpose) or predict the mean (for regression purpose) of an individual tree. The RF reduces the risk of overfitting by averaging the outputs of individual decision trees and ensures that it generalizes well to the unseen data. This is particularly important in case of an AM process, where slight variations in process parameters can lead to significant changes in the deposition quality. The strength of the RF lies in its ability to handle *complex* and *non-linear relationships* between the input and output parameters. The RF algorithm is particularly useful when numerous interacting features exist, for example in case of μ-PMAM process in which multiple deposition parameters such as μ-plasma power, deposition head traverse rate, and feedstock powder flow rate interact in a non-linear manner to influence the deposition geometry.
- **K-Nearest Neighbours (KNN):** It is a simple, instance-based ML algorithm that makes predictions based on the proximity of data points. It works by identifying the K-nearest neighbours of a test data and then using their values to predict the output. Its output is based on either the majority class (for classification purpose) or the average of the nearest data points (for regression purpose). The proximity of the specified data points allows the KNN algorithm to effectively capture the local variations in deposition height and width in an AM process. But, KNN can be computationally expensive for large datasets because it requires calculating the distance between training data and test data.

- **Support Vector Regression (SVR):** It is a regression-based ML algorithm that uses support vectors to find the best fit curve within a specified margin. It aims to find the balance between its complexity and prediction accuracy by minimizing the error within a specified margin. This makes it more generalizable algorithm.
- **LASSO Regression:** It is a linear regression-based ML algorithm that uses L1 regularization to shrink the coefficients of less important features to zero thus effectively performing feature selection. This algorithm is beneficial when dealing with the large datasets that have many features because it helps to identify the most relevant features for predicting the targeted output.
- **Ridge Regression (RR):** It uses L2 regularization which penalizes large coefficients without eliminating any features. This ML algorithm helps to minimize overfitting by ensuring that the coefficients remain small and does not fit the noise in the datasets.
- **Gaussian Process Regression (GPR):** It is a non-parametric, probabilistic ML algorithm that uses a kernel function to capture the underlying function and predict outputs with uncertainty estimates. It is particularly useful for *complex* and *non-linear relationships* between input and output parameters. It is well-suited for scenarios where the data are noisy or where uncertainty in the predictions needs to be quantified.

1.1.3 Applications of ML in Manufacturing

The ML finds applications in many areas because it adapts well and works. It is used to spot the trends in experimental data, simulate complicated physical systems, and speed up the simulations. Its μ-plasma power to handle complex, unorganized, and massive datasets makes it a very promising alternative when the standard statistical algorithms fail. Following are some specific applications in of ML in manufacturing:

- **Industry 4.0:** ML can play a major role in Industry 4.0 because it allows intelligent automation and uses data to assist in the decision making. As factories and systems handle huge data and become more intricate, engineers find ML to boost productivity, make systems more reliable, and bring fresh ideas to a company.
- **Predictive maintenance**: ML analyzes sensor data from machines to predict potential failures before their occurrence. This reduces unexpected downtime, lowers maintenance costs, and improves the overall reliability and lifespan of a manufacturing equipment.
- **Process optimization**: ML can optimize process parameters in real-time by analysing the performance data. This results in more efficient production, accurate geometry, reduced material wastage, and better use of energy and the resources. This enhances the productivity and reduces the cost.

- **Quality control**: The ML can detect the manufacturing defects or irregularities using sensor signals or images. This enables automated inspection and ensures that only high-quality products reach the next stage thus improving consistency and reducing rework and scrap.
- **Supply chain management**: ML can improve demand forecasting by analyzing historical and real-time data thus helping to maintain an optimum inventory levels. This enhances planning, reduces storage costs, and increases responsiveness to the fluctuations customer demands or the market.
- **Energy management**: ML can help manufacturers to adjust operations for better efficiency by analyzing an equipment usage and its energy consumption patterns. It enables the system to recommend the changes that reduces energy costs maintaining the same productivity.

1.1.4 Applications of ML in Additive Manufacturing

Following are some major applications of ML in AM processes:

- **Parametric optimization**: ML can find the optimum combination of an AM process parameters such as μ-plasma power, deposition material supply rate, deposition head traverse rate, stand-off-distance, and similar other parameters. Such optimized combination results in better surface quality, desired deposition geometry, and more consistent properties of the manufactured product.
- **Defect prediction and detection**: ML can identify different defects such as porosity, warping, cracking, etc. produced by an AM process by using the real-time data or thermal imaging. Early detection of such defects reduces the material and energy wastage and ensures better quality of the manufactured product.
- **Process monitoring**: ML can continuously monitor the important AM process parameters such as temperature, layer thickness, and feedstock material flow. This ensures that any deviations are quickly addressed which improves an AM process performance and consistent quality of the manufactured products.
- **Material characterization**: ML can expedite discovery of new materials by identifying patterns in its large experimental datasets. It helps to predict material behavior, saving time and reducing the number of the required tests.
- **Geometric accuracy enhancement**: ML can predict the potential shape distortions during in an AM process and can suggest the real-time corrections. This helps to maintain the dimensional accuracy of a manufactured product thus reducing necessity for its post-processing. It also ensures a product is manufactured as per its original design.

1.2 Deep Learning

DL is a subset of ML which relies on the neural networks having many layers to recognize the complicated patterns. DL can identify the features from the raw data which ML cannot do. The DL algorithms rely on an input layer, several hidden layers, and an output layer of the neural networks. Neurons in these layers transform the information and send it onward. The term "deep" indicates many hidden layers in the neural networks, which help them to learn the complex details. The DL algorithms work well with the supervised learning but also work with the semi-supervised and unsupervised learning also. Autoencoders and generative adversarial networks are techniques of the unsupervised learning (**Zhang and Zhang, 2023)**. Training methods such as backpropagation and stochastic gradient descent adjust the weights of the neural networks to improve their prediction accuracy. DL is useful for extensive and high-dimensional datasets. It is playing a key role in many industries to solve various problems.

1.2.1 Types of Deep Learning Algorithms

Following are the commonly used DL algorithms:

- **Convolutional Neural Networks (CNN):** They are used to handle and study the *visual information* by having several hidden layers which make them to learn how to spot the patterns, features, and shapes in the images. The CNN works well with the tasks of classifying images, detecting objects, and splitting images into parts because they pick up the spatial hierarchies. Different filters are used before the CNN which scan the input images to locate the edges, form, and detailed patterns. This makes CNN very useful in the applications that demand accuracy and speed in the visual datasets.
- **Recurrent Neural Networks (RNN):** They are μ-plasma powerful DL algorithm that are designed to handle *time-series* or sequential data. The core idea behind RNN is that they maintain an internal state (memory) that is updated at each time step based on the input received. The output at each time step depends not only on the current input but also on the information retained from previous time steps. It implies that the recurrent connections use the previous inputs in a sequence to influence how the RNN process the current and future inputs. This cyclic structure allows them to learn the *patterns* and *relationships* over the *different time durations*. The RNN rely on time sequential updating of the hidden layers at every run. The RNN combine this with the current input to generate an output while also updating themselves for the next input. This characteristic makes them useful for the manufacturing processes where past inputs influence future outputs, such as in multi-layer deposition by an AM process, where the deposition parameters of one layer are influenced by those of the previous layer.

- **Bidirectional Long Short-Term Memory (Bi-LSTM):** Bi-LSTM is an advanced version of the standard LSTM, which is designed to capture long-term dependencies in time-series data in a better manner by processing them both in forward and backward passes i.e., input data are processed from the 1st hidden layer to the last hidden layer in the forward pass and then the same data are processed from the last hidden layer to the 1st hidden layer in the backward pass. This lets Bi-LSTM to work with both past and future context at the same time which improve the performance. Unlike regular RNN, LSTM have a memory cell that can store information for long periods, allowing them to retain relevant information over multiple time steps. Bi-LSTM are useful in areas like *speech recognition*, *text classification*, and *machine translation* where the meaning of a word depends on the words around it. The bidirectional approach of Bi-LSTM allows it to learn from both past and future data points thus providing a more comprehensive understanding of the temporal patterns in the deposition process. This is particularly beneficial in multi-layer deposition, where the relationship between layers is not only dependent on previous layers but may also be influenced by subsequent ones.
- **Self-Attention Temporal Convolutional Networks (SA-TCN):** They combine convolutional layers with a self-attention mechanism, making them highly effective at capturing both local and long-range dependencies in time-series data. This hybrid approach allows SA-TCN to focus on critical features of the data across different time durations regardless of their temporal distances. In the context of multi-layer depositions, this means that this algorithm can consider how each layer deposition characteristics such as height, width, and deposition material flow affect the characteristics of subsequent deposition layer, leading to more accurate predictions.

1.2.2 Applications of DL in Manufacturing

- **Visual inspection:** DL uses computer vision to identify surface defects, scratches, or deformations with high accuracy. It automates quality inspection, reduces human error, and ensures consistent product quality for large production volumes.
- **Robotics:** DL enables robots to adapt to changing environments using visual and sensor data. This improves flexibility in tasks like sorting, assembly, and navigation, especially in unstructured or unpredictable environment.
- **Predictive modelling:** The complex algorithms of DL forecast outcomes such as machine failures or product quality. These algorithms handle non-linear relationships and large datasets, offering more accurate predictions than traditional ML algorithms.
- **Speech and language processing:** DL supports voice-controlled manufacturing systems by understanding commands through natural language processing. This

improves human-machine interactions, simplifies operations, and increases productivity on the shop floor.

- **Fault Diagnosis:** DL processes sensor signals to detect patterns that indicate machinery faults. It identifies early warning signs of failure, allowing preventive maintenance and reducing unexpected downtime in manufacturing systems.

1.2.3 Applications of DL in Additive Manufacturing

- **Layer-wise Defect Detection:** DL algorithms analyse images or sensor data layer-by-layer during multi-layer deposition by an AM process. It detects defects such as inter-layer porosity and dimensional inaccuracy on real-time basis, enabling immediate corrective actions and improving final quality of a manufactured product.
- **Process optimization:** DL optimizes AM process parameters by predicting outcomes, reducing defects, improving selection of parameters, and enhancing deposition quality through data-driven analysis and real-time process control.
- **Real-time control:** DL enables dynamic adjustment of deposition parameters during an AM process. This adaptive control improves stability, reduces errors, and ensures consistent part geometry and material quality throughout manufacturing process.
- **Prediction of material properties:** DL algorithms analyse past process and material data to estimate mechanical properties such as strength and hardness. This helps in quality confirmation of the manufactured products without excessive testing.

1.3 Additive Manufacturing

Additive manufacturing (AM) is revolutionizing the manufacturing world, transforming the way products are designed, developed, and made in different industries. This technique builds three-dimensional objects by depositing material layer by layer using the bottom-up approach unlike the casting processes in which material is deposited in bulk and the machining processes which remove the material from a solid block using the top-down approach. AM starts with a digital 3D model of a product. Special software then slices it into thin horizontal layers. The AM machine gets these layers as instructions. It then it deposits the material to match the product design. The raw material can be a polymer, metal, alloy, ceramic, composite, or biopolymers. The choice depends on intended application of a product. AM gives the designers more freedom and boosts efficiency.

1.3.1 Classification of AM Processes

According to ASTM F42, different AM processes are categorized into the following seven categories as shown in Fig. 1.5:

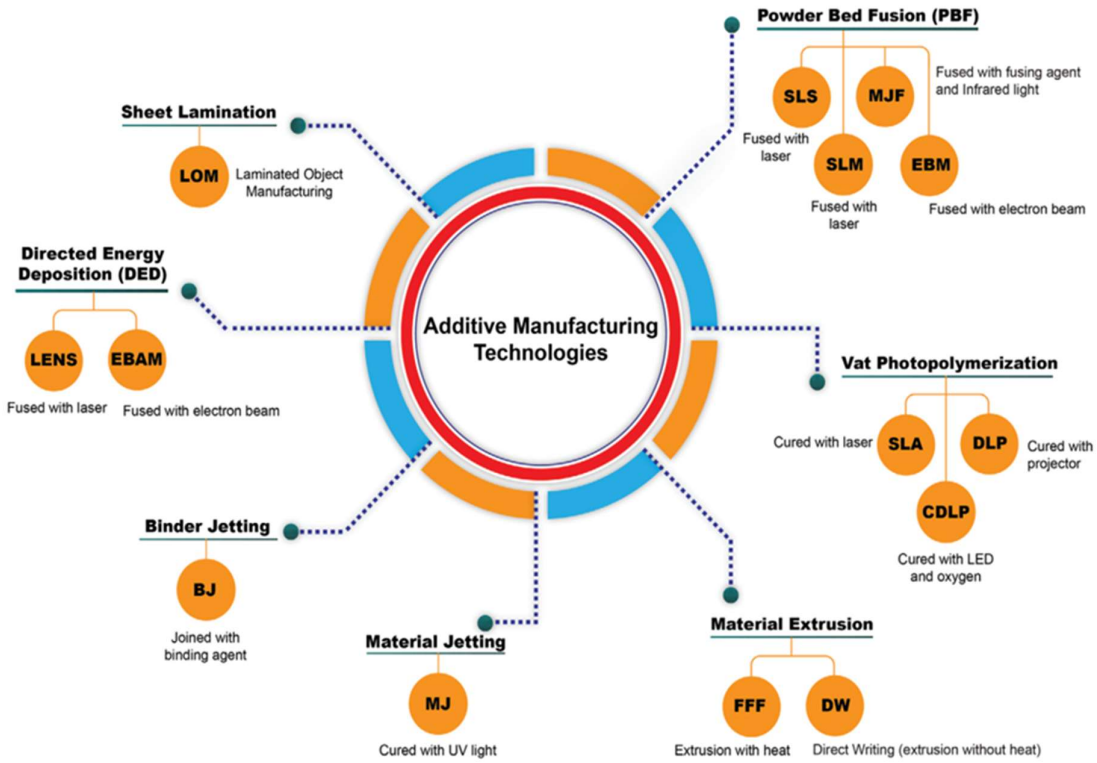

Fig. 1.5: Classification of AM processes according to ASTM F42 **(Rafiee et. al. 2020).**

- **Powder Bed Fusion (PBF):** PBF type AM processes use heat source in the form a laser or electron beam to selectively fuses regions of the powdered bed of the feedstock material which is either metallic material or a polymer. Electron Beam Melting (EBM), Selective Laser Sintering (SLS), Selective Laser Melting (SLM), Direct Metal Laser Sintering (DMLS), Selective Heat Sintering (SHS), and Multi Jet Fusion (MJF) are common AM processes in this category. They differ based on the materials they use and how much melting takes place during the process. The PBF processes have ability to integrate at small scale and they are used for AM of relatively large products. Their machines are of large size. But, built speed is relative slow, they require high µ-plasma power, and their surface finish depends on the powder size
- **Directed Energy Deposition (DED):** DED type AM processes use the concentrated heat source in the form a laser, electron beam, plasma arc, or µ-plasma arc to melt and fuse the feedstock material as is being deposited. The feedstock material is a metallic material which can be supplied either in powder form or wire form or combination of the both. These AM processes produce high quality functional products, perform precise repair of the existing components, add complex features to the pre-fabricated parts, produce and restore high-value engineering components, and fabricate near-net-shape products. Their build speed is often sacrificed for higher accuracy. The DED fabricated products require post-processing to achieve the desired quality. Laser Engineering Net

Shape (LENS), Laser Metal Deposition (LMD), Wire-arc Additive Manufacturing (WAAM), and μ-plasma Metal Additive Manufacturing (μ-PMAM) are the commonly used DED type AM processes.

- **Sheet Lamination:** Sheet lamination type AM processes bond together the sheets or foils of different metallic materials, papers or fabrics using heat, adhesives, or ultrasonic waves to supply the required bonding energy. A laser, or milling machine is used to make products from the laminated sheets. Laminated Object Manufacturing (LOM) and Ultrasonic Additive Manufacturing (UAM) are the commonly used sheet lamination type AM processes. These processes offer high build speed, low cost, ease of material handling, higher accuracy, and good finish.
- **Binder Jetting:** In binder jetting type AM processes, a liquid bonding agent is selectively deposited to join powder of feedstock material (either a metallic material or a polymer) thus binding them to create a solid layer. When one layer is finished, the platform moves down, and new powder is added on top. This cycle repeats until the full object is completely built. Powder Bed and Inkjet Head (PBIH) and Plaster-based 3D Printing (PP) are the commonly used binder jetting type AM processes. Advantages of these processes include: faster process, high range of materials, allows use of two materials, use of different colours. Their major limitations are: not always suitable for structural parts due to use of binder material, and higher amount of post processing
- **Material Jetting:** Material jetting involves depositing droplets of the feedstock material (usually photopolymers or waxes) onto a build platform, where they are immediately solidified by UV light. This process is similar inkjet printing in 3D. Advantages of material jetting type AM processes include: high accuracy, less wastage of materials, ability to fabricate multi-materials and multi-colours products thus making them ideal for visual prototypes and biomedical models. But they require support structures and are applicable to limited range of materials only. Multi-jet Modelling (MJM) is the most commonly used material jetting type AM process.
- **Material Extrusion:** This process uses a nozzle or orifice to selectively extruded the feedstock material to form its layers. The nozzle moves along the x and y axes to deposit material onto a base, while the platform shifts along the z-axis to create the product layer by layer. Common materials feedstock materials are thermoplastics or thermoplastic composites. It is used to fabricate inexpensive parts from ABS or some other plastics, Extrusion type AM processes are relatively inexpensive, suitable for the visual models and prototypes. But they have low accuracy, small build speed, limited nozzle radius,

requires constant pressure of the feedstock material. Fused Deposition Modelling (FDM) is the most commonly used material extrusion type AM process.

- **Vat Photopolymerization:** This type AM processes selectively cure a liquid photopolymer by exposing it to the light from a laser or projector to produce its solid layers via light-activated polymerization process. The build platform begins at the bottom of a container filled with liquid photopolymer. A light source hardens it based on its cross-section being exposed, solidifying it as it moves up. Stereolithography apparatus (SLA) and Digital Light Processing (DLP) are the commonly used vat polymerization processes. These processes are relatively quick and typically build large areas. But, they relatively expensive, requires support structure, require higher post-processing time and cost, and are applicable to limited material i.e. photopolymers only.

1.3.2 Advantages of AM Processes

AM processes offer a series of distinctive benefits that set them apart from conventional manufacturing processes:

- **Geometrical freedom:** AM enables the fabrication of highly complex products that are unattainable through traditional processes such as casting, forming, powder metallurgy, or machining processes. This capability allows for the realization of intricate free-form designs with minimal constraints.
- **Digitally driven production:** Since AM is governed by digital designs therefore it enables precise reproduction of the optimized geometries. The integration of computer-aided design with automation ensures high precision, dimensional control, and repeatability across multiple production cycles.
- **Tailored multi-material fabrication:** AM processes support integration of diverse materials within a single build cycle, facilitating development of the advanced materials such as smart composites, functionally graded materials, and bio-compatible materials. This flexibility contributes to innovation in material science.
- **Assembly reduction:** The layered deposition mechanism of AM processes permits direct fabrication of complicated and integrated assemblies. This eliminates the need to manufacture and later assemble multiple parts, thereby improving product integrity and reducing the likelihood of mechanical failures due to misalignment caused in the assembly process.
- **Autonomous manufacturing:** AM equipment can produce intricate, multi-material parts with minimal human intervention. This autonomy enhances manufacturing efficiency and allows for decentralized on-demand production closer to the point of use.

- **Material efficiency:** In contrast to conventional subtractive manufacturing processes, which often remove excess material from a larger stock, AM adds material only where it is required. This approach minimizes scrap, reduces material costs, and eliminates the need for extensive cutting tools or fixtures.
- **Economical customization:** Unlike traditional manufacturing, which relies heavily on moulds and dies, AM can produce customized parts directly from a digital file without any tooling. This feature is highly valuable in sectors requiring patient-specific implants, customized surgical tools, or bespoke heritage restoration components.
- **Environmental sustainability:** AM processes contribute positively to environmental sustainability by lowering material wastage and energy consumption. Precise deposition and reduced reliance on tooling also help in diminishing the carbon footprint associated with manufacturing.

1.3.3 Limitations of AM Processes

Despite its numerous advantages and potentials, AM continues to face following major technological and practical challenges:

- **Material limitations:** Current AM systems are typically compatible with a limited range of materials. Many machines are optimized for metals, polymers, wax, composites with specific thermal and mechanical properties. AM of ceramics, and integration of dissimilar materials within a single machine remains a significant hurdle, demanding further research in material compatibility and hybrid process development.
- **Production speed and scalability:** While AM is well-suited for customized, low-volume production, it remains less efficient for mass production. The relatively slow build speed limits its suitability for large-scale manufacturing applications, especially where throughput is critical.
- **Accuracy constraints:** The additive nature of AM introduces challenges in achieving tight dimensional tolerances and smooth surface finish. Layering artifacts, commonly referred to as the “stair-stepping” effect, are particularly evident on curved surfaces and intricate geometries.
- **Requirement for post-processing:** Parts produced via AM often require secondary operations such as machining, heat treatment, or polishing to meet the functional and aesthetic standards. These additional steps add to the production time and cost, making the overall process less efficient than initially perceived.
- **Data intensity and computational demand:** Generating and processing highly complex geometries through AM involves big data and intricate toolpath algorithms. The demand for robust computational μ-plasma power and efficient slicing software

continues to be a significant bottleneck, especially for parts with fine internal features or lattice structures.

1.3.4 Applications of AM Processes

Since its emergence in late 1990s, AM has undergone significant advancements and has been increasingly adopted across various sectors. Following are some of its transformative applications:

- **Biomedical engineering:** AM is reshaping the biomedical field by enabling the creation of accurate anatomical parts, orthopaedic implants, dental restorations, and surgical instruments. The ability to produce patient-specific devices using certified bio-compatible materials is revolutionizing surgical planning, medical education, and implantology.
- **Aerospace industry:** Aerospace manufacturers have been early adopters of AM, utilizing its ability to reduce component weight, consolidate parts, and improve performance. Applications include rocket engine components, combustor liners, interior cabin parts, and ducting systems for environmental control. AM supports design innovation while meeting stringent strength and thermal requirements.
- **Consumer goods:** AM is employed in product development for consumer electronics, household appliances, and sporting goods. Designers benefit from rapid prototyping capabilities, allowing quick iterations and product validation before full-scale manufacturing. As the technology matures, it is poised to support larger production runs in consumer markets.
- **Energy sector:** AM contributes to the energy industry by enabling the production of complex, high-performance components such as turbine nozzles, pump manifolds, and control-valves. These components are often subjected to extreme operating conditions, and AM allows for material and design customization to meet specific environmental demands.
- **Transportation:** The transportation sector leverages AM to develop lightweight, aerodynamic, and heat-resistant components for automotive and rail systems. Applications include ductwork, grilles, interior modules, and structural panels that reduce vehicle weight and enhance performance at high speeds.

1.4 Directed Energy Deposition (DED) Processes

The DED type AM processes are integral to the field of AM due to their distinct advantages and versatile capabilities. These processes stand out for their ability to deposit a wide range of materials, such as metals, alloys, composites, and even ceramics, offering exceptional adaptability to various industrial applications. This broad material compatibility makes DED processes highly relevant in the sectors ranging from aerospace to automotive, where customized solutions are essential. A key benefit of DED technology is its ability to achieve high deposition rates, which translates to faster build times compared to other AM techniques. Particularly when large volumes of material are required, DED processes enable more efficient production, significantly reducing manufacturing time. This enhanced productivity positions DED as a compelling choice for industries facing stringent production deadlines and the need for rapid turnaround times. Moreover, DED processes are especially valuable for repair and cladding applications. Sectors such as aerospace, oil and gas, and automotive often rely on DED for this purpose, as it allows for the repair of high-value parts without the need for complete replacement. The flexibility of DED in these applications demonstrates its significant role in prolonging the lifespan of critical components. Additionally, DED processes can be easily scaled to produce large components and structures. This scalability ensures that DED is not limited to small parts but can also accommodate the production of sizable, complex structures. Its capacity to handle large-scale fabrication further enhances its appeal for industries that require both precision and the production of substantial parts. In terms of design flexibility, DED provides engineers and designers with the freedom to produce the parts with complex geometries and intricate features. This capability fosters innovation and supports the development of custom solutions tailored to specific needs, pushing the boundaries of what is possible in modern manufacturing. Such flexibility is a significant advantage, enabling the creation of highly specialized components that would be difficult or impossible to achieve through traditional manufacturing methods. Finally, DED processes are known for their material efficiency. By adding material only where it is needed, these processes minimize material wastage and reduce associated costs. This level of efficiency is especially advantageous compared to other AM techniques and conventional manufacturing processes which often result in higher material wastage. Material efficiency of DED aligns with growing emphasis on sustainability in manufacturing making these processes as environmentally friendly choice.

1.4.1 Types of DED Processes

The DED processes are classified based on type of energy source and feedstock material:

- **Wire Arc Additive Manufacturing (WAAM):** These processes use an arc to melt and layer metallic wires onto the base surface. It uses different types of arcs such as manual metal arc (MMA), gas metal arc (GMA), or gas tungsten arc (GTA) to supply the heat for melting the metallic wires. The WAAM processes have high build speed which can create large parts from inexpensive metals though they produce poor surface quality. Aerospace and marine industries use WAAM to make structural large parts, where cost-cutting and time-saving are important factors.
- **Laser-Based DED (L-DED):** A laser beam heats and melts the metallic powder or wire before adding it to a base surface. This process works by directing the laser beam onto the base where it melts the material so it can bond with the surface or with earlier layers. L-DED processes (i.e., LENS, LMD) provide great control and accuracy during the deposition process. They let manufacturers make complex shapes with precision. Many industries such as aerospace, automotive, and tooling use this approach to create prototypes, fix broken parts, or produce parts close to their final shape.
- **Plasma Arc Additive Manufacturing (PAAM):** These processes use a plasma or μ-plasma arc to heat and melt metallic powders or wires for their deposition on a base surface. Plasma or μ-plasma arc is created through gases such as argon or nitrogen by applying direct current (DC) μ-plasma power supply. This produces a high-temperature plasma jet that melts the feedstock material. The molten material is then deposited on the base surface in layered manner fabricate the desired part. The PAAM allows fast material deposition and creates strong metallurgical bonds. It works well for making high-performance parts needed in the fields such as aerospace, defence, and energy.

1.4.2 Advantages of DED Processes

The primary advantage of DED processes comes from how flexible it is with materials. It works with metals, alloys, ceramics, and even composites, making it useful in a variety of applications. These processes let users combine materials with different properties in the same build. This helps in creating graded materials, smart materials, biocompatible materials, high/medium entropy alloys or ones with specific mechanical, thermal, or electrical properties. WAAM and PAAM processes give high deposition rates. This makes them capable of making large components and lowering both production time and costs. It also provides impressive design freedom, making it possible to create complicated parts with detailed features. Engineers and designers can use this to deliver unique solutions and parts customized for specific needs. DED processes are used to repair or clad the parts, which helps extend the life of essential components while cutting down on maintenance expenses.

1.4.3 Limitations of DED Processes

The DED processes also suffer from certain drawbacks which need attention. One of the challenges is dealing with residual stresses and distortions in the fabricated parts using high-energy laser beams or plasma arcs. Designers and engineers need to optimize these processes to reduce these issues and maintain accuracy in dimensions and part quality. Another challenge lies in additional processes such as machining, grinding, or heat treatments needed to achieve smooth surfaces, precise dimensions, or the required texture. These extra steps slow down the production and increase productions costs. Improvements in process monitoring and control are reducing how much post-processing is necessary.

1.4.4 Applications of DED Processes

DED processes find applications in many industries such as aerospace, automotive, biomedical, defence, oil and gas, chemical, tooling. Aerospace companies rely on DED processes to make intricate structural parts, engine components, and fix turbine blades. Automotive industries use them to speed up prototyping to create tools and customize the parts. Defence industries use DED processes to build lightweight armour, make missile parts, and fix military vehicles. Oil and gas industries use DED processes to create tough coatings, repair drilling equipment, and produce downhole tools. Dies and mould making industries use DED processes to create cores, inserts, and intricated cavity components.

1.5 Micro-plasma Metal Additive Manufacturing (μ-PMAM)

μ-PMAM process is a novel and energy-efficient metal AM process that combines the principles of μ-plasma arc with the precision of modern material deposition methods. It represents a significant advancement in the field of DED, especially in applications that demand fine control, and minimal thermal impact. By using μ-plasma arc as low-energy, highly concentrated thermal source as the heat source, μ-PMAM is capable of producing high-quality components from high-melting point metallic materials. The μ-plasma arc is generated inside a specially designed nozzle unlike the PAAM process. The nozzle controls the arc size and intensity, ensuring focused heating and efficient material deposition. Unlike conventional PAAM process, μ-PMAM operates at lower current and μ-plasma power levels, usually up to 20 amperes and 440 Watts DC μ-plasma power. These controlled energy settings offer several benefits, such as reduced heat-affected zones, minimized thermal distortion, and lower residual stresses within the deposited layers. One of the distinguishing features of μ-PMAM process is its integration with 5-axis computer numerically controlled (CNC) work table. Fig. 1.5 depicts photograph of the 5-axis CNC machine for μ-PMAM process showing the deposition head and formation of μ-plasma arc inside the μ-plasma torch in the insets. This configuration allows for the fabrication of

geometrically complex parts without any support material. The multi-axis motion enables the deposition head to be pregummed for the desired part geometry thus allowing overhangs, internal features, and curved geometries to be manufactured more easily. Consequently, µ-PMAM offers superior flexibility and freedom in part design, reducing the need for post-processing and support removal. A major advantage of µ-PMAM lies in its compatibility with multiple feedstock forms including powders, wires, or their combinations. This versatility allows users to select the most appropriate form of feedstock material based on part requirements, desired deposition rate, or economic considerations. For instance, powder feedstock offers better control over composition and microstructure, while wire feedstock provides better material utilization and reduced contamination risk. From a materials perspective, µ-PMAM is highly capable of handling a broad range of high-performance and high-melting-point alloys many of which are difficult to process by other AM processes. The µ-PMAM process has been successfully used for Inconel 625 for high-temperature aerospace applications, P20 and H13 tool steels for mould and die production, and Stellite alloys for wear-resistant surfaces, Ti6Al4V, Co-Cr-Mo-xTi, Ti-Ta-Zr-W-Mo HEA for biomedical implants, and Ti6Al4VxNiyCr for high strength applications. The precise control over heat input and deposition rate allows for stable melting and solidification of challenging materials which helps to expand its material applications. These materials are selected for their mechanical and biological properties, making them ideal for implants, surgical instruments, and prosthetic components.

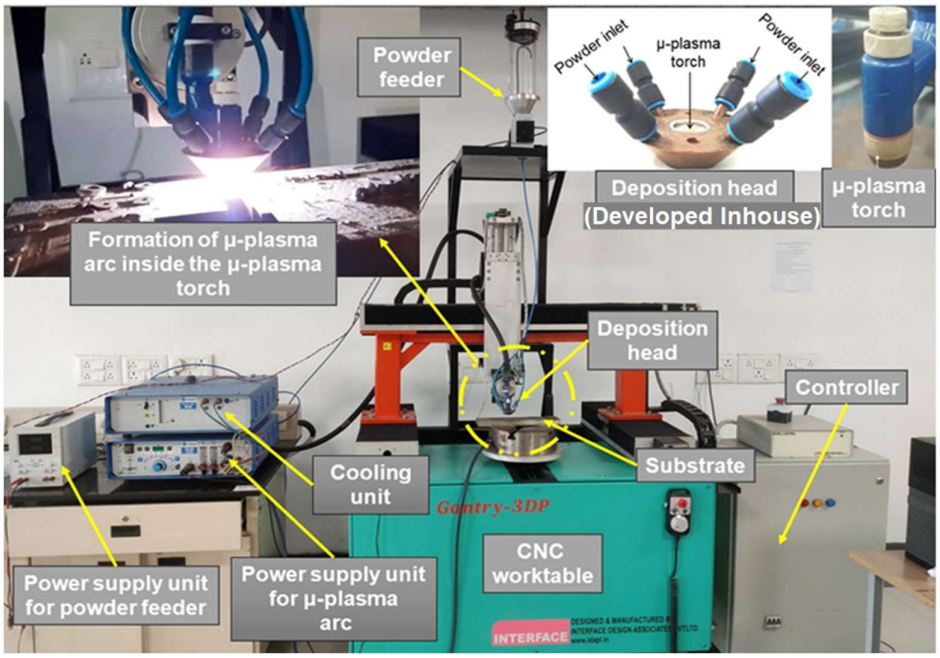

Fig. 1.6: Photograph of the 5-axis CNC machine for µ-PMAM process showing the deposition head and formation of µ-plasma arc inside the µ-plasma torch in the insets.

In terms of functional outcomes, the parts produced through μ-PMAM often exhibit fine-grained microstructures, uniform layer bonding, and high mechanical strength due to controlled thermal cycles and precise deposition paths. Its ability to handle custom geometries and specialized materials opens new possibilities for repairing, re-manufacturing, and customizing critical components. This is especially relevant in high-value sectors namely aerospace, automotive, biomedical, and defence where performance, reliability, and material efficiency are critical

1.5.1 Applications of μ-PMAM Process

- **Aerospace components:** μ-PMAM enables fabrication of complex, lightweight parts using high-temperature alloys such as Inconel 625, offering superior heat resistance, geometric precision, and reduced material waste for turbine blades and aerospace brackets.
- **Tools and dies manufacturing:** The μ-PMAM process efficiently produces and repairs moulds of P20 and H13 materials enhancing their useful life, reducing lead time.
- **Biomedical implants and devices:** The μ-PMAM process has been used to process biocompatible materials such as Ti6Al4V, Co-Cr-Mo-xTi, Ti-Ta-Zr-W-Mo with tailored microstructures, allowing the production of patient-specific implants and surgical tools with improved mechanical and biological performance.
- **Development of high-entropy alloy:** It μ-PMAM process has been used to develop advanced alloys such as Ti6Al4VxNiyCr, Co-Cr-Mo-xTi, Ti-Ta-Zr-W-Mo, enabling components with superior strength, corrosion resistance, and biocompatibility for demanding structural and biomedical applications.
- **Component repair and remanufacturing:** μ-PMAM process can repair worn or damaged high-value metallic parts by adding material only where needed, extending component life and reducing replacement costs and environmental waste.

1.6 Organization of thesis

This thesis is organized into the following five chapters:

Chapter 1 introduces the fundamentals of machine learning (ML) and deep learning (DL). It describes main types of ML and DL algorithms. It highlights applications of ML and DL in manufacturing and additive manufacturing (AM) for detection of defects, quality control, and parametric optimization. It provides an overview of different types of AM processes, their advantages, limitations, and key industrial applications. It briefly introduces directed energy deposition (DED) processes and Micro-Plasma Metal Additive Manufacturing (μ-PMAM) process, summarizing their principles, key benefits, and major applications.

Chapter 2 reviews the relevant literature on use of ML and DL in AM, emphasizing previous work on process optimization, defect detection, and deposition geometry control in DED, WAAM, and μ-PMAM processes. It present the research gaps identified based on this review, and research objectives identified based upon the research gap along with the methodology used to meet them.

Chapter 3 details the materials and research methodology used in this study, including the selection of deposition materials, data acquisition through video recording, feature extraction, and preparation of datasets. It describes the training and evaluation of various ML and DL algorithms for predicting deposition geometry and outlines the integration of these algorithms with the NSGA-II algorithm for multi-objective optimization.

Chapter 4 presents the results and discussion, including performance of different ML and DL algorithms in predicting deposition geometry for single-layer and multi-layer depositions respectively. It analyzes performance of the selected ML and DL algorithm, the effectiveness of NSGA-II in optimizing process parameters, and the optimized parameters for both single-layer and multi-layer depositions.

Chapter 5 summarizes the outcome of the present research by presenting its significant achievements, conclusions, and some directions for the future work.

Chapter 2

Review of Past Work

This chapter presents review of the past work carried out on application of ML and DL to perform different tasks such as detection and minimization of defects, prediction and control of deposition geometry, and parametric optimization in metallic AM (MAM) processes such as DED, WAAM, and μ-PMAM. It also presents summary of the past work review, existing research gaps, identified research objectives along with the methodology used in the present work to achieve them.

2.1 Past Work on ML Usage in AM Processes

Optimization of a MAM processes involves detection and elimination or minimization of deposition defects, achieve accurate deposition geometries, and adjusting its parameters to improve the build quality. In recent years, ML and DL have become increasingly popular for optimizing the MAM processes, for example, ML and DL have been used for L-DED, WAAM, and LPBF processes to enhance their outcomes. Following sections describe the review of the past work performed to detect and minimize deposition defects and to optimize deposition geometry using ML/DL.

2.1.1 Detection and Minimization of Deposition Defects Using ML/DL

Deposition defects such as porosity, lack of fusion, cracks, and delamination in a MAM process can severely compromise mechanical properties of the fabricated product therefore their early detection and mitigation are crucial. And use of ML/DL for detecting and minimizing these defects has been one major research thrust.

Some researchers have used ML algorithms in the DED processes for monitoring and reducing the deposition defects by exploiting open architecture of DED processes where the melt pool is visible during deposition which allows for diverse sensor integration. **Khanzadeh et *al.* (2018)** applied clustering algorithm to sensor data in L-DED process to detect out-of-distribution process events without needing the labelled data. **Montazeri et *al.* (2019)** combined ML algorithm with optical emission spectroscopy in a DED process and showed that spectral patterns of the plume can predict the defects. **Liu et *al.* (2022)** used high-speed video monitoring of the melt pool in the laser wire additive manufacturing (WLAM) process and extracted feature descriptors to train the Naïve Bayes ML algorithm for detection of the defects. Their study could identify the defects such as humping (i.e., irregular bead formation) and lack-of-fusion on real-time basis. Some researchers have utilized vision-based and hybrid ML algorithms to tackle the defects such as pores, cracks, and geometric irregularities in the WAAM process. **Tang et *al.* (2020)** used ML-DL

combined two-stage approach to detect the welding defects such as burn-through and poor deposition continuity in the robotic WAAM process. Their approach involved analysis of weld pool images by neural networks to identify defect precursors which is supplemented by the support vector machine (SVM) classifier for final defect categorization. **Zhang et *al.* *(*2023)** used YOLO-based detector to the x-ray images of WAAM fabricated multi-layer deposition for identification of pore defects in it.

Some researchers have leveraged in-situ monitoring data such as optical images, infrared thermal videos, acoustic signals in combination with DL algorithms to identify the deposition defects on real-time basis or post-MAM process. **Scime and Beuth (2018)** used the CNN to classify anomalous regions on layer images and successfully detected spatter-induced porosity and other irregularities in the LPBF process. **Yuan et *al.* (2018)** demonstrated that high-resolution visual imaging of the powder bed in the LPBF process can feed the DL algorithms to flag the defects such as recoated blade interference or uneven powder distribution. **Baumgartl et *al.* (2020)** used infrared thermography data as input to a DL algorithm and correlated formation of porosity with the thermal patterns in LPBF process. Some researcher used DL-based closed loop control to minimize the defects. Some researchers have used DL-based closed loop control to minimize the defects. **Kwon et *al.* (2020)** implemented closed-loop control in a L-DED process in which DL algorithm was trained to recognize the impending defects (like bead misalignment or instability) from real-time sensor data, and the system automatically adjusted process parameters (e.g., laser μ-plasma power or deposition head traverse rate) to avoid occurrence of the defects. Their study demonstrated feasibility of coupling DL-based diagnostics with immediate corrective actions which will reduce defect occurrence. **Wang et *al.* (2023)** proposed a real-time defect detection framework for LPBF process using a vision-based DL algorithm to monitor each deposition layer and to pause process if a serious anomaly is detected.

2.1.2 Deposition Geometry Optimization Using ML/DL

Another critical aspect in the MAM processes is achieving the desired deposition geometry in terms of optimized deposition width and height, total height, and overall dimensional accuracy of a deposition. Controlling these geometrical parameters is especially important in DED and WAAM processes where melt pool dynamics and heat accumulation can lead to irregular layer profiles. Traditional approaches for parameter setting namely trial-and-error method or physics-based algorithms are often time-consuming or may not capture complex interactions between multiple parameters of an MAM process. Thus, researchers are increasingly exploring different ML/DL algorithms to predict and optimize deposition geometry through optimization of the process parameters

with a goal of identifying optimum settings that yield the target geometry. Such data-driven algorithms effectively serve as surrogates for an MAM process, enabling optimization of layer geometry without exhaustive physical experimentation.

Researchers have used ML algorithms in WAAM process for deposition geometry prediction due to its relevance in producing large structural components with relatively coarse deposition geometry. **Chandra et al. (2024)** conducted a comparative evaluation of multiple ML algorithms to predict the deposition height and width in a WAAM process using stainless steel wire. They trained ML algorithms using a dataset comprising of travel speed, wire deposition head traverse rate, torch angle, and stand-off distance as inputs. They achieved reasonably high accuracy in estimating the deposition dimensions. They reported that a simple linear regression ML algorithm performed better for deposition width prediction whereas a non-linear ML algorithm was more accurate for deposition height prediction. It highlights that the appropriate ML algorithm may be different for different geometric features of a deposition. **Subadra et al. (2024)** utilized ML algorithms to predict deposition geometry and recommended process parameter settings for deposition width and height of stainless steel depositions by WAAM process by examining the effects of voltage, current, travel speed, and wire deposition head traverse rate. They reported that the random forest ML algorithm reliably predicted deposition dimensions from the process parameters, and an inverse prediction used the KNN to suggest the process parameter settings that are likely to produce the desired shape of a deposition. Some researchers have shown that ML algorithms can capture the relationship between laser μ-plasma power, scan speed, powder deposition head traverse rateand the resulting melt pool dimensions in the LDED process. **Xiong et al. (2019)** developed an ANN to predict total height of multi-layer depositions by LDED process which will help to select parameters that yield a uniform height. **Zhang et al. (2021)** integrated a vision system that measured the cross-sectional profile of a deposition in real-time and fed these measurements into a controller tuned by ML which adjusted the travel speed to maintain a targeted deposition width. These approaches illustrate the extension of ML from purely predictive use to active control for geometry stabilization in LDED process.

The layer geometry in the LPBF process is dictated by powder spreading and melt pool behaviour at much finer scale therefore the focus of deposition geometry optimization is different. ML/DL has been used in LPBF process to ensure uniform layer deposition and to predict distortions or dimensional deviations after depositing. **Grill et al. (2019)** used ML to optimize scan path or pattern in LPBF process to achieve uniform energy distribution, which indirectly ensures consistent melt track geometry and layer thickness. **Ren et al.**

(2021) applied a DL algorithm to predict the final part distortion in LPBF process for given a set of process parameters and scan strategies, thereby guiding parameter selection to minimize the warping. **Kumar and Jain (2022)** employed a KNN algorithm to predict the surface roughness of multi-layer depositions built by μ-PMAM process. They used the feedstock material in both powder and wire form and the ML algorithm could forecast the resulting surface roughness from process inputs with reasonable accuracy (within ~6% error). **Mukherjee et al. (2020)** achieved a reduction in bead height variance in WAAM deposition. **Liu et al. (2022)** demonstrated more uniform build walls in a DED process as compared to baseline settings.

2.2 Summary of Past Work Review

Following is the summary of the review of past works on usage of ML/DL algorithms in MAM processes:

- There is growing use of ML and DL in AM processes for detection of defects, predicting deposition geometry, and process optimization especially in MAM processes such as DED, WAAM, and LPBF processes.
- ML can map subtle process signals such as video, spectra, etc. in the DED processes to defect occurrence of defects thus providing early warning for the quality deviations.
- Supervised DL algorithms, especially CNN, are effective in recognizing the defects from the complex sensor data i.e., images and thermal fields in the PBF processes. Even for the comparatively coarse features of WAAM (as opposed to fine powder beds), modern DL can successfully pinpoint internal and surface defects (including small pores or inclusions) with high confidence.
- ML-based closed-loop or adaptive control are still in early stages but they highlight the trend from defect analysis towards in-situ defect minimization using ML.
- ML/DL algorithm when properly trained and validated can effectively predict how changes in parameters of an MAM process will affect the deposition geometry. This capability greatly accelerates process optimization, enabling practitioners to attain the desired deposition dimensions and mechanical properties linked to geometry also, with fewer experimentations. It also leads to a common theme that use of ML as a μ-plasma powerful tool to navigate multi-parameter process for desired geometric outcomes.
- From the initial demonstrations of CNN classifying defects from the images of an MAM process, the research is moving towards a sophisticated multi-sensor data fusion and even preliminary autonomous control for quality assurance in the AM processes. These advances provide a strong foundation for improving reliability in MAM processes via intelligent, data-driven monitoring.

2.2 Identified Research Gaps

Following are the research gaps identified from review of the past work:

- No work is available on ML/DL based geometry prediction of single and multi-layer depositions fabricated by μ-PMAM process using their real-time data
- No work is available on multi-objective optimization of μ-PMAM process parameters with conflicting objectives
- No work is available on real-time, closed-loop systems that will not only detect but also minimize or eliminate defects in the μ-PMAM process.

2.3 Research Objectives

The following are the research objectives (RO) of the present work based on some of the identified research gaps:

- **RO-1: Selection of an appropriate ML algorithm** which is capable of accurately predicting deposition height and width of single-layer depositions by μ-PMAM process on the same material base plate using the real-time data extracted from their high-resolution video recordings. The selected ML algorithm to be trained, validated and tested using the real-time data only.
- **RO-2: Selection of an appropriate DL algorithm** which is capable of accurately predicting total height and width of multi-layer depositions by μ-PMAM process on the mild steel base plate using the real-time data extracted from their high-resolution video recordings. The selected DL algorithm should be capable of handling increased nonlinearity can capture inter-layer dependency, and spatial and sequential dependencies in the multi-layer depositions.
- **RO-3: Multi-objective optimization of μ-PMAM process parameters** (i) using the selected ML algorithm integrated with the non-dominated sorting genetic algorithm II (NSGA-II) for the single-layer depositions to identify optimum combinations of process parameters that will yield the desired deposition geometry, and (ii) using the selected DL algorithm integrated with NSGA-II for the multi-layer depositions to handle the added complexity and to identify optimum combination of process parameters that will achieve uniform and defect-free deposition across multiple layers.

2.4 Research Methodology

Fig. 2.1 shows schematic of the research methodology to meet the identified objectives of the present work.

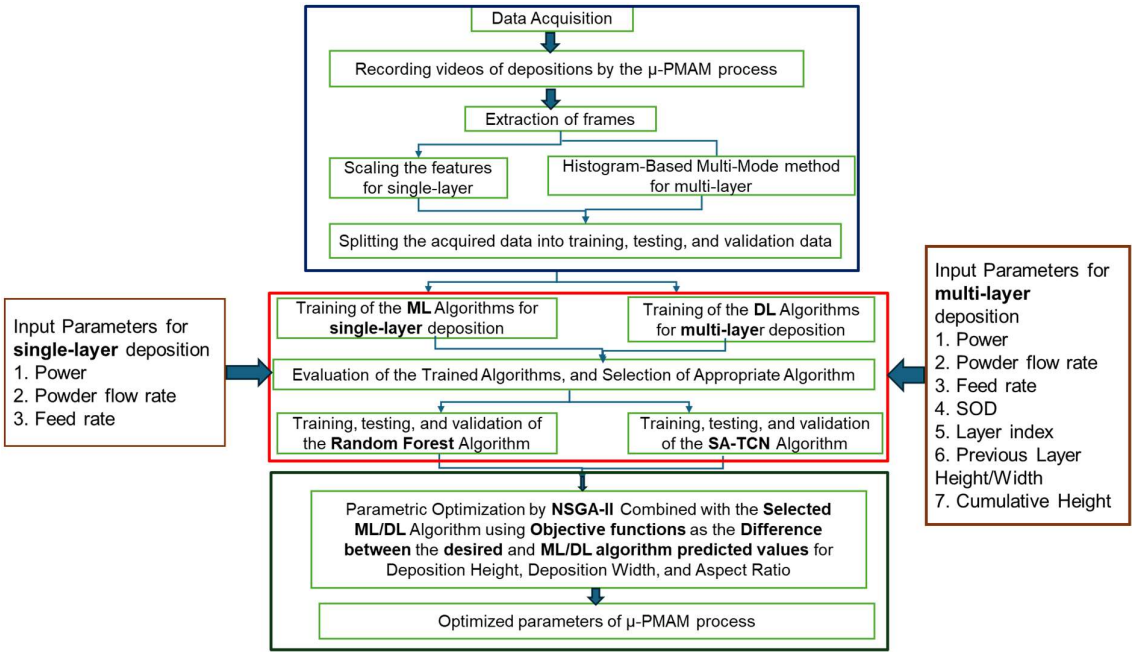

Fig. 2.1: Research methodology used in the present work.

The used research methodology involves several key steps, starting from data acquisition to training of ML and DL algorithms, followed by multi-objective optimization of process parameters for optimum deposition geometry by integrating the selected ML and DL algorithm with the NSGA-II. It begins with recording videos of single and multi-layer depositions fabricated by μ-PMAM process using a high dynamic range camera. The recorded videos were broken down into individual images to extract relevant information image-wise. The prepared datasets were split into training, testing, and validation sets for the considered ML and DL algorithms. Six ML algorithms and three DL algorithms were trained and evaluated for single-layer and multi-layer depositions respectively. All trained ML and DL algorithms were evaluated using coefficients of determination, mean average error (MAE) to select the appropriate algorithm. The algorithm selection process involved evaluating the 6 ML and 3 DL algorithms based on their predictive accuracy, generalizability, and suitability for the characteristics of the available datasets. The selected ML and DL algorithm were trained, validated and tested using the real-time data. These algorithms can quickly predict the height and width of the deposition for any set of input parameters. The selected ML algorithm was integrated with the non-dominated sorting genetic algorithm II (NSGA-II) for multi-objective optimization of the single-layer depositions to identify optimum combinations of process parameters that will yield the desired deposition geometry. While, selected DL algorithm was integrated with NSGA-II for multi-objective optimization of the multi-layer depositions to identify optimum combination of process parameters that will achieve uniform and defect-free deposition

across multiple layers. The ML/DL integrated NSGA-II yielded several sets of optimized parameters (i.e., μ-plasma power, deposition head traverse rate, feedstock feedstock powder flow rate) that can give desired geometry.

This chapter presented a review of the relevant literature, identified research gaps, research objectives of the present work along with the methodology used to meet them. The **next chapter** describes details of the materials for single layer and multi-layer depositions, data acquisition through recording of videos, processing of these videos, training, validation, testing and evaluation of the considered ML and DL algorithms, training of the selected ML and DL algorithm, and multi-objective optimization of by μ-PMAM process parameters by selected ML and DL algorithm integrated with NSGA-II for the single-layer and multi-layer depositions.

Chapter 3

Materials and Methods

This chapter details the deposition materials used in this study, data acquisition through video recording, feature extraction, and preparation and splitting of the datasets. It also describes training, validation, testing and evaluation of the considered ML and DL algorithms, training of the selected ML and DL algorithm, and multi-objective optimization of by μ-PMAM process parameters by selected ML and DL algorithm integrated with NSGA-II for the single-layer and multi-layer depositions.

3.1 Selection of Deposition and Base Plate Materials

Table 3.1 presents details of the deposition and base plate materials used for fabricating single-layer and multi-layer depositions by μ-PMAM process.

Table 3.1: Deposition and base plate materials used in single-layer and multi-layer depositions by μ-PMAM process.

Layer	Deposition material	Base plate material
Single-layer depositions	Ti6Al4V	Ti6Al4V
Multi-layer depositions	SS 316L	Mild steel

The SS 316L is an austenitic stainless steel whose composition by wt.% is: 16-18% Cr; 10-14% Ni; 2-3% Mo; Max. 0.03% C; and small amounts of Manganese, Silicon, and other elements. The 'L' indicates very less carbon content. It has excellent resistance to atmospheric corrosion, moderately oxidizing and reducing environments, chloride-rich environments, good strength and toughness, even at cryogenic temperatures, good weldability. Its main applications include: (i) Biomedical devices due to its biocompatibility and resistance to corrosion, (ii) Marine environments for structural components and equipment exposed to seawater, (i) Food processing due to its resistance to corrosion and non-toxicity, (iv) Chemical and petrochemical industries for equipment handling corrosive chemicals, and (v) Cryogenic applications due to its ability to maintain strength at very low temperatures. The Ti-6Al-4V, sometimes also called TC4 or Ti64 , is an alpha-beta titanium alloy of ASTM Grade 5. Its composition by wt.% is: 5.5-6.75% Al; 3.5-4.5% V; 0.3% Fe; 0.2%O; 0.08% C; 0.05% N; 0.015%H; and balance Ti. It has excellent biocompatibility, excellent corrosion resistance to seawater, oxidizing acids and rocket propellants, relatively low density and thermal conductivity, high strength and modulus of elasticity, and good fatigue strength and formability. It is primarily used in various aerospace applications, orthopaedic implants because it promotes bone regeneration, and high-temperature components. Therefore, these two materials were chosen the deposition materials.

3.2 Selection of Input Parameters

The performance of the μ-PMAM process is highly dependent on the input parameters. These parameters directly influence the deposition geometry, including height, width, and consistency of the deposited layers. Different combinations of the following input parameters were used during video recording of the single-layer depositions of Ti6Al4V to capture their effects on the deposition geometry thus allowing the ML algorithms to learn their relationships with the deposition geometry:

- **μ-plasma power:** The energy supplied for formation μ-plasma arc inside the μ-plasma torch. It affects the time required to melt a deposition material and form a cohesive layer. Higher the μ-plasma power, lesser is the time needed to melt a deposition material.
- **Feedstock powder flow rate:** It is the rate at which the feedstock or deposition material is delivered to the base plate. It influences height and width of a deposition. It depends on density, particle size and sticking tendency of feedstock powder. Its value is restricted by μ-plasma power i.e., smaller value of μ-plasma power does not allow use of larger value of feedstock powder flow rate.
- **Deposition head traverse rate:** It is speed at which the deposition head travels over the base plate. Its value is affected by melting point of the feedstock material and μ-plasma power. Higher melting of the feedstock material and/or smaller value of μ-plasma power necessitates small traverse rate of deposition head and vice-versa. It affects geometry of a deposition layer and overall deposition quality.

In addition to the above-mentioned parameters, following additional input parameters, as depicted in Fig. 3.2, were used for multi-layer depositions of SS 316L to account for the increased complexity:

- **Stand-Off-Distance (SOD):** The distance between the nozzle and the substrate, which affects the material deposition angle and consistency.
- **Layer Index *'N'*:** It indicates which layer is being deposited.
- **Height and width of previous layer (PreLH and PreLW):** The height and width of the previously deposited layer is important because it provides the immediate context for deposition of the next layer.
- **Cumulative deposition height *'CumH'*:** The cumulative height of all previously deposited layers directly reflects their consistency and quality. A consistent value of CumDH indicates that the material is being deposited uniformly, which is essential for providing a stable base for the next layer.

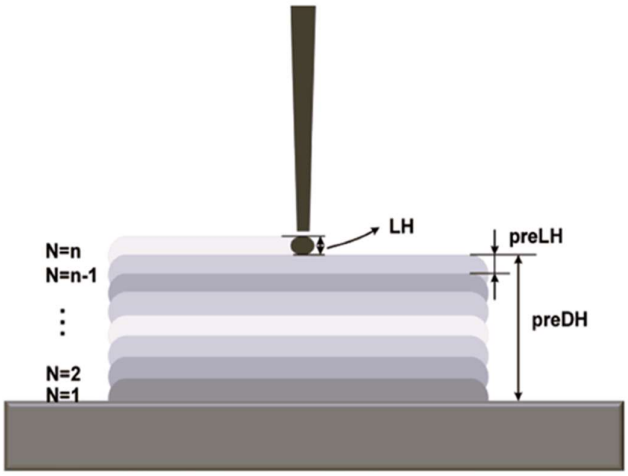

Fig. 3.1: Additional inpur parameters for a multi-layer depositon.

3.3 Data Acquisition

Data acquisition plays an important role in training, validation, testing, and evaluation of ML and DL algorithms. The data were acquired by extracting the images from the recorded videos by a high dynamic range (HDR) camera (Make: TPS, Model: XVC-1000-1100) mounted on the CNC machine of the μ-PMAM process as shown in Fig. 3.1. This HDR camera was selected for its ability to capture high-resolution video with enhanced lighting sensitivity. Video recording of the deposition process at a high image rate made it possible to observe the deposition geometry in real-time and capture any subtle variations that could influence the final part quality. Following high-quality grey videos were recorded for different combination of μ-plasma μ-plasma power and deposition head traverse rate: (i) 8 videos for single-layer depositions of SS 316L on mild steel base plate, (ii) 2 videos for single-layer depositions of Ti6Al4V on mild steel base plate, (iii) 6 videos for single-layer depositions of Ti6Al4V on same material base plate, and (iv) 4 videos for multi-layer of SS 316L on mild steel base plate. Table 3.2 provides details of these recorded videos. They provide real-time visual insights into the deposition process allowing for extraction of deposition height and width. The data collected through this method was crucial for the data-driven ML and DL algorithms that can forecast the deposition geometry and optimize the process parameters.

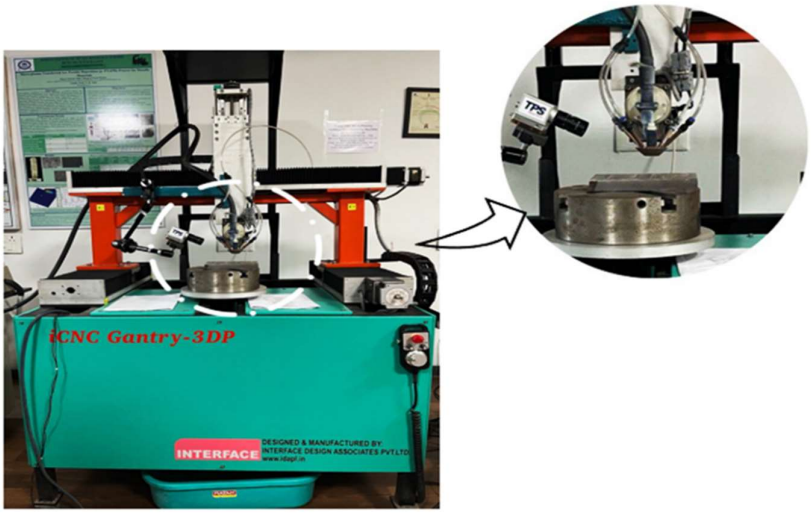

Fig. 3.2: Photograph of the CNC machine of μ-PMAM process showing mounting of the high dynamic range (HDR) camera of make TPS XVC-1000-1100.

Table 3.2: Details of recorded videos for single-layer and multi-layer depositions by μ-PMAM process.

Video No.	Deposition material	Base plate material	No. of layers	μ-plasma power (W)	Deposition head traverse rate (mm/min)	Feedstock powder flow rate (g/min)	Duration of the recorded video (seconds)	Number of extracted images
1	SS 316L	Mild steel	Single-layer	308	47	1.7	66	60
2					50	2.1	54	48
3					53	3.5	62	49
4				319	47	2.5	71	64
5					53	2.1	62	52
6				330	47	1.5	69	59
7					50	1.7	68	60
8					53	1.9	61	52
9	SS 316L	Mild steel	4	308	53	1.8	180	120
10			6	308	53	2.5	348	290
11			6	308	53	2.3	243	220
12			6	319	50	1.8	173	160
13	Ti6Al4V	Mild steel	Single-layer	330	55	1.5	60	55
14				330	55	2.1	11	10
15	Ti6Al4V	Ti6Al4V	Single-layer	330	50	2.7	8	6
16				330	50	2.9	440	380
17				330	50	2.1	23	20
18				330	50	1.7	56	43
19				330	55	3.5	59	51
20				374	50	2.3	80	30

3.4 Processing of the Recoded Videos

Processing of the recoded videos is needed to ensure that ML and DL algorithms receive clean and well-structured data that can lead to their accurate predictions. Therefore, the recorded videos were processed in the following steps: (i) Extraction of images from each

recorded video, (ii) Scaling of features for single-layer depositions data, (iii) Histogram-based multi-modal method for multi-layer depositions, and (iv) careful splitting of each dataset into training, testing, and validation subsets.

3.4.1 Extraction of Images from the Recorded Videos

Image extraction from a recorded video is a key step in transforming the visual data into a usable information for the ML and DL algorithms. Therefore, images were extracted from each recorded video whose details are provided in Table 3.1. The image extraction process was performed using Python-based image processing tool ensuring that the entire process is efficiently carried out without human intervention. Each extracted image provides details of the deposition geometry at a specific point in time, capturing critical features such as deposition height and width. The extracted images were then analysed and processed further to extract meaningful features that were used for training the ML and DL algorithms. The extracted images were then labelled based on the deposition parameters (i.e., μ-plasma μ-plasma power, deposition head traverse rate, and feedstock powder flow rate) used while recording a particular video. This labelling allowed for the establishment of a direct relationship between the input parameters and the observed deposition geometry.

3.4.2 Feature Scaling for Single-Layer Depositions Data

Data having input features or parameters with varying scales affect performance of ML algorithms due to their sensitivity towards the scale of input features. Therefore, feature scaling was applied to the extracted real-time data of single-layer depositions to standardize the input parameters. Standardized scaling was chosen for this study in which standard value of an input parameter was computed using the Eq. 1. It transforms the data so that each parameter has a mean of 0 and a standard deviation of 1 ensuring that all input parameters are treated equally by an ML algorithm regardless of their original scales and prevent it from being biased toward parameters with larger magnitudes. For example, μ-plasma power ranges from 100 W to 440 W whereas, deposition head traverse rate could vary from 5 to 20 mm/s, and feedstock powder flow rate might range from 0.2 to 1.5 g/min. Without standardization, the ML algorithm could disproportionately focus on μ-plasma power due to its wide numerical range than that of the deposition head traverse rate or feedstock powder flow rate. But, use of standardized scaling transformed all these input parameters to a comparable scale so that an ML algorithm treats them equally regardless of their original scales without being biased toward the parameters with larger magnitude. Therefore, standardization of input features is crucial for improving the predictive accuracy of an ML algorithm because it allows it to effectively learn the relationships between these parameters and the resulting deposition geometry.

$$x' = \frac{x - \mu}{\sigma} \quad (1)$$

where, x' are *'x'* are standardized and original value respectively of an input parameter; *'μ'* and *'σ'* are mean and is standard deviation of that parameter. Table 3.3 presents real-time data generated from the recorded videos of single-layer depositions of Ti6Al4V by μ-PMAM process after removing all those data which yielded same values of deposition width and height. These data were used in training, validation, and testing of six ML algorithms.

Table 3.3: Real-time data generated from recorded video of single-layer deposition of Ti6Al4V and used in training, validation, and testing of the six ML algorithms.

Data no.	μ-plasma power (W)	Feedstock powder flow rate (g/min)	Deposition head traverse rate (mm/min)	Deposition width (mm)	Deposition height (mm)	Aspect ratio	Quality of deposition
1.	330	1.7	50	2.94	1.65	1.78	CUD
2.	330	2.1	55	2.96	1.76	1.68	CUD
3.	330	2.1	55	2.99	2.00	1.50	CUD
4.	330	1.7	50	2.89	1.42	2.04	NUD
5.	330	2.1	55	3.12	1.53	2.04	NUD
6.	330	2.7	50	3.10	1.60	1.94	NUD
7.	374	2.3	50	4.08	3.13	1.30	NUD
8.	330	2.1	55	4.23	2.89	1.46	CUD
9.	330	2.9	50	4.38	3.19	1.37	NUD
10.	330	1.5	55	4.45	3.31	1.34	NUD
11.	330	1.5	55	4.29	2.93	1.46	CUD
12.	330	3.5	50	4.37	3.14	1.39	NUD
13.	330	2.1	55	4.01	2.63	1.53	CUD
14.	374	2.3	50	4.11	2.87	1.43	CUD
15.	330	2.9	50	4.57	2.74	1.67	CUD
16.	330	3.5	50	4.61	2.97	1.55	CUD
17.	330	1.5	55	4.37	2.45	1.78	CUD
18.	330	1.5	55	4.49	2.64	1.70	CUD
19.	374	2.3	50	4.11	3.37	1.22	NUD
20.	330	2.1	55	3.94	2.97	1.33	NUD
21.	330	2.9	50	1.6	3.05	0.53	NUD
22.	330	3.5	50	1.92	2.83	0.68	CUD
23.	374	2.3	50	1.54	3.09	0.50	CUD
24.	374	2.3	50	1.92	3.03	0.63	CUD
25.	374	2.3	50	1.57	2.81	0.56	CUD
26.	330	1.5	55	2.97	1.84	1.61	NUD
27.	330	1.5	55	1.95	3.25	0.60	NUD
28.	330	2.3	50	1.97	2.83	0.70	NUD
29.	330	2.9	50	1.66	2.74	0.61	CUD
30.	330	1.5	55	1.62	2.81	0.58	CUD
31.	330	1.5	55	1.99	2.99	0.67	CUD
32.	330	2.1	50	2.69	1.71	1.57	NUD
33.	330	1.7	50	2.66	1.59	1.67	NUD
34.	330	2.1	50	2.68	1.72	1.56	NUD
35.	330	2.1	50	2.67	1.68	1.59	CUD
36.	330	1.7	50	2.13	2.78	0.77	CUD
37.	330	2.1	55	2.08	2.73	0.76	CUD
38.	330	2.1	55	2.18	2.79	0.78	NUD
39.	330	1.7	50	1.66	2.74	0.61	CUD
40.	330	1.7	50	3.32	2.05	1.62	CUD

*****NUD: non-uniform deposition; CUD: continuous and uniform deposition*

3.4.3 Histogram-Based Multi-Modal Method for Multi-Layer Depositions

The traditional analysis methods for geometry of a multi-layer deposition primarily focus on calculating the average height and width over a predefined deposition length. Though these methods are simple and efficient but it has a significant limitation that it overlooks the local variations within the deposition process. By relying only on average values, the traditional methods fail to capture the fluctuations in deposition height and width that may occur at various points along the deposition length. These local variations are important as they affect quality, uniformity, and performance of multi-layer depositions.

A new *histogram-based multi-modal method* introduced in this study in which deposition height and width are measured at regular interval of 1 mm along the deposition length from the recorded video of a multi-layer deposition. Analysis of the deposition geometry data at such a small interval ensures more accurate and comprehensive understanding of the deposition process. It will not only identify the average values of deposition geometry data but also captures the local variations and inconsistencies that are missed in the traditional methods of deposition geometry analysis. Generation of histogram-based data for a multi-layer deposition requires the following steps to be performed:

- **Normalization of data:** Measured values of height and width of a particular layer of a multi-layer deposition are normalized by using Eqs. (2) and (3) to ensure that the data are comparable for different deposition layers:

$$h_i' = \frac{h_i - \mu_h}{\sigma_h} \tag{2}$$

$$w_i' = \frac{w_i - \mu_w}{\sigma_w} \tag{3}$$

  where, *'h_i'* and *'w_i'* re the values of height and width of a particular deposition layer of a multi-layer deposition measured on the i^{th} location along the deposition length and h_i' and w_i' are their normalized values for *i = 1, 2, 3, ... n*; *'n'* is total number of measured data for height or width for each deposition layer; ' μ_h' and $'\sigma_h'$; and $'\mu_w'$and $'\sigma_w'$ are the mean and standard deviation of the dataset for deposition height and width of a particular layer of a multi-layer deposition respectively.

- **Histogram generation data:** Histogram data are generated for height and width of each layer of a multi-layer deposition using their normalized values. The x-axis of a histogram represents value of deposition width or height with a tolerance range of ±0.2 mm and its y-axis show frequency or occurrence for each value.

- **Identification of modes:** The generated histogram data for height and width of each layer of a multi-layer deposition are divided into three regions by calculating % distribution of data using Eq. 4.

$$P_j = \frac{Frequency\ of\ Occurrence\ of\ j^{th}\ value}{n} \times 100 \quad (4)$$

where, *'P_j'* is percentage of occurrence of j^{th} value of height or width of each layer of a multi-layer deposition; and *'n'* is total number of measured data for height or width for each deposition layer. Primary, secondary, and tertiary modes are identified based on the computed distribution of values. The *primary mode* represents the most common values of deposition height or width occurring along the deposition length. It corresponds to the regions where the deposition process is the most consistent producing deposition height and width remaining stable at 60 to 70% of the deposition length. The *secondary* and *tertiary modes* represent the regions where the local variations in deposition height and width occur along the deposition length. These variations may be due to slight fluctuations in process parameters such as μ-plasma power, deposition head traverse rate, feedstock powder flow rate, and stand-off distance which affect the deposition geometry at specific locations. Secondary and tertiary modes together represent 30–40% of value of deposition height or width occurring along the deposition length.

Table 3.4 presents the histogram-based data generated from the recorded video number 10, 11, and 12 (as mentioned in Table 3.2) for 6 layers of 3 multi-layer depositions of SS 316L by μ-PMAM process. The percentages associated with each value of deposition height or width in Table 3.4 represent the percentage of deposition length over which a particular value of deposition width or height of deposition layer lies within a tolerance range of ±0.2 mm. For example, if the primary mode represents 65%, it means that 65% of the deposition length has a consistent height and width around this value, indicating a stable deposition process. The remaining 35% may consists of fluctuations (represented by secondary or tertiary mode) or gaps (zero values) thus revealing the values over which the deposition process is less consistent or interrupted. It implies that these data offer valuable insights into the deposition characteristics and performance. The data of Table 3.4 will be used for training the three DL algorithms.

Table 3.4: Histogram-based real-time data generated from the recorded videos of multi-layer depositions of SS 316L and used in the training, validation, and testing of three DL algorithms.

Layer index '*N*'	µ-plasma power	Deposition head traverse rate	Feed-stock powder flow rate	SOD (mm)	CumH (mm)	PreLH (mm)	PreLW (mm)	Height #1 (% occurrence along the deposition length)	Height #2 (% occurrence along the deposition length)	Height #3 (% occurrence along the deposition length)	Width #1 (% occurrence along the deposition length)	Width #2 (% occurrence along the deposition length)	Width #3 (% occurrence along the deposition length)
Video number: 10													
1	308	53	2.5	12	0	0	0	3.71 (63.91%)	3.12 (28.05%)	4.23 (8.05%)	3.96 (63.87%)	4.52 (30.07%)	5.02 (6.06%)
2	308	53	2.5	12	3.71	3.71	4.12	3.74 (63.49%)	3.1 (18.25%)	4.48 (18.25%)	4.10 (63.27%)	3.60 (18.36%)	5.24 (18.36%)
3	308	53	2.5	12	7.45	3.74	4.14	3.67 (63.44%)	3.02 (18.28%)	4.42 (18.28%)	3.90 (64.44%)	3.41 (17.78%)	5.20 (17.78%)
4	308	53	2.5	12	11.12	3.67	4.11	3.46 (67.41%)	3.0 (16.30%)	4.39 (16.30%)	3.95 (63.64%)	3.45 (18.18%)	5.15 (18.18%)
5	308	53	2.5	12	14.64	3.46	4.1	3.70 (64.71%)	3.12 (17.65%)	4.33 (17.65%)	4.10 (63.7%)	3.55 (18.14%)	5.34 (18.14%)
6	308	53	2.5	12	18.1	3.70	4.04	3.70 (62.16%)	2.97 (18.92%)	4.20 (18.92%)	4.18 (63.72%)	3.67 (18.14%)	4.76 (18.14%)
Video number: 11													
1	308	53	2.3.	8	0	0	0	3.34 (76.52%)	2.90 (11.85%)	4.46 (11.63%)	3.86 (50.85%)	4.35 (39.26%)	3.16 (9.89.%)
2	308	53	2.3	8	3.34	3.34	3.86	3.35 (66.93%)	2.87 (22.7%)	4.47 (10.37%)	3.82 (51.37%)	4.30 (30.82%)	3.17 (17.81%)
3	308	53	2.3	8	6.69	3.35	3.82	3.29 (62.8%)	3.83 (25.74%)	4.43 (11.46%)	3.86 (60.11%)	4.42 (30.89%)	3.17 (9.0%)
4	308	53	2.3	8	9.98	3.29	3.86	3.29 (59.77%)	3.78 (28.12)	4.44 (12.11%)	3.78 (55.26%)	4.45 (24.68%)	3.08 (20.06%)
5	308	53	2.3	8	13.27	3.29	3.78	3.38 (66.54%)	3.98 (22.57)	4.51 (10.89%)	3.79 (67.09%)	4.38 (20.17%)	3.18 (12.74%)
6	308	53	2.3	8	16.65	3.38	3.79	3.27 (72.92%)	3.76 (16.21%)	4.39 (10.87%)	3.74 (62.43%)	4.49 (30.94%)	3.17 (6.2%)
Video number: 12													
1	319	50	1.8	10	0	0	0	3.33 (58.0%8)	2.80 (21.0%)	3.80 (21.0%)	3.94 (70.81%)	3.24 (14.59%)	4.66 (14.59%)
2	319	50	1.8	10	3.33	3.33	3.94	3.45 (71.53%)	3.02 (14.23%)	3.98 (14.23%)	3.94 (70.17%)	3.34 (14.91%)	4.98 (14.91%)
3	319	50	1.8	10	6.78	3.45	3.94	3.41 (66.27%)	2.98 (16.87%)	4.12 (16.87%)	3.87 (71.41%)	3.25 (14.3%)	4.82 (14.3%)
4	319	50	1.8	10	10.19	3.41	3.96	3.54 (59.54%)	3.05 (20.23%)	4.10 (20.23%)	3.87 (70.89%)	3.20 (14.55%)	4.92 (14.55%)
5	319	50	1.8	10	13.73	3.54	3.87	3.46 (60.28%)	2.95 (19.86%)	3.97 (19.86%)	3.96 (70.89%)	3.50 (14.55%)	4.78 (14.55%)
6	319	50	1.8	10	17.19	3.46	3.96	3.43 (58.77%)	2.99 (20.61%)	3.96 (20.61%)	3.93 (71.08%)	3.40 (14.46%)	4.99 (14.46%)

3.3.4 Splitting of Datasets

The generated real-time data for single-layer deposition (Table 3.3) and multi-layer depositions (Table 3.4) were split into three subsets namely training, validation, and testing datasets in ratio of 70:20:10. The training data were used to train ML or DL algorithms, allowing them to learn the relationships between input parameters and deposition geometry. The validation data were used to fine-tune the hyperparameters of ML or DL algorithms and ensure that they did not overfit the training data. Finally, the testing data were used to

evaluate performance of ML or DL algorithms by providing an unbiased assessment of their predictive accuracy.

3.5 Selection and Training of ML Algorithms for Single-Layer Depositions

Six ML algorithms namely Random Forest (RF), K-Nearest Neighbours (KNN), Support Vector Regression (SVR), Gaussian Process Regression (GPR), LASSO Regression, and Ridge Regression were chosen for prediction of deposition geometry for single-layer depositions. Following are justifications for their selection: (i) Strength of the RF algorithm lies in its ability to handle *complex* and *non-linear relationships* between the input and output parameters. It is particularly useful when numerous interacting features exist, for example, the μ-PMAM process in which multiple deposition parameters such as μ-plasma power, deposition head traverse rate, and feedstock powder flow rate interact in a non-linear manner to influence the deposition geometry, (ii) Proximity of the specified data points allows the KNN algorithm to effectively capture the local variations in deposition height and width in an AM process such as μ-PMAM process, (iii) Key advantage of SVR is its ability to effectively capture *non-linear relationships* between the input parameters and the targeted output parameters, (iv) GPR algorithm is particularly useful for *complex* and *non-linear relationships* between input and output parameters. It is well-suited for scenarios where the data are noisy or where uncertainty in the predictions needs to be quantified, (v) LASSO and Ridge regression algorithms are useful in dealing with the large datasets that have many features because they identify the most relevant features for predicting the targeted output. The selected ML algorithms were trained and validated using the earmarked 70% and 20% of the real-time data respectively (presented in Table 3.3) for single-layer deposition of Ti6Al4V by μ-PMAM process and algorithm-specific parameters as presented in Table 3.5. The real-time data of Table 3.3 possess diverse deposition scenarios with variations in key process parameters whereas parameters in Table 3.5 offer valuable insights into the configurations used for each ML algorithm for its best performance.

Table 3.5: Parameters related to the six ML algorithms used in the present study.

ML Algorithm name	Parameter	Value
Random Forest	n_estimators	500
K-Nearest Neighbours	K	5
Support Vector Regression	Kernel	RBF
	C	1000
Gaussian Process Regression	Kernel	C [1, (0.01, 0.1)] x RBF [1, (10^{-3}, 10^{3})]
LASSO Regression	Alpha	0.02
Ridge Regression	Alpha	1

Number of estimators used for the training of RF algorithm was 500 using real-time data for single-layer deposition, capturing a broad range of deposition scenarios. Value of '*K*' as 5 was used training the KNN algorithm implying that it considered the 5 nearest neighbours to predict the deposition geometry. The SVR algorithm employed radial basis function (RBF) as kernel with a regularization parameter C as 1000. This parameter controls trade-off between fitting the data and maintaining simplicity of the algorithm. It helps to prevent overfitting by penalizing the excessively complex algorithms that fit the noise in the data rather than the true underlying trend. The kernel used in GPR is a combination of C [1, (0.01, 0.1)] and RBF kernel with a parameter range from 10^{-3} to 10^{3}. This kernel choice allows this algorithm to capture both smooth variations and sharp changes in the deposition process. The alpha parameter for the LASSO algorithm was set to be as 0.02 which controls strength of the regularization. A larger value of alpha would result in more features being eliminated whereas its smaller value would allow more features to contribute to the LASSO algorithm. The alpha parameter for Ridge Regression algorithm was set equal to 1, balancing the trade-off between fitting the data and maintaining algorithm simplicity.

3.6 Selection and Training of DL Algorithms for Multi-Layer Deposition

Three DL algorithms namely Recurrent Neural Network (RNN), Bidirectional Long Short-Term Memory (BiLSTM), and Self-Attention Temporal Convolutional Network (SA-TCN) were chosen for predicting the deposition geometry of multi-layer deposition. These algorithms were chosen because they are adept at capturing the complex temporal dependencies between deposition layers in a multi-layer deposition, where the characteristics of a previously deposited layer influence the next deposition layer. The chosen DL algorithms were trained via the Adam optimizer with a learning rate of 0.001 and a batch size of 32 for 100 epochs using the earmarked 70% and 20% of the histogram-based data respectively (presented in Table 3.4) for multi-layer depositions of SS 316L by the μ-PMAM process. Two hidden layers with 128 nodes in each hidden layer were used in the training of RNN algorithm along with a dropout rate of 0.2 to prevent the overfitting. The BiLSTM algorithm, which demonstrates improved performance in capturing long-range dependencies, was trained using 64 nodes in each direction. Training of the SA-TCN algorithm employed 4 temporal convolutional layers with kernel size of 3, 64 filters per layer, and a multi-head self-attention mechanism having 4 heads to enhance the learning of contextual dependencies.

3.7 Evaluation of the Trained ML and DL Algorithms

The trained ML and DL algorithms were evaluated or tested by predicting deposition height and deposition width for single-layer and multi-layer depositions by feeding the

earmarked 10% of input data of Table 3.3 and Table 3.4 respectively having different parametric combinations of μ-plasma power, deposition head traverse rate, and feedstock powder flow rate. The predictions by the ML and DL algorithms offer valuable insights into their ability to generalize across different deposition conditions. It reveals how accurately the algorithms could predict the deposition height and width, as well as other critical parameters, for both known and new data. Furthermore, they help to identify any patterns or systematic errors, enabling further refinement of the ML and DL algorithms for improved prediction accuracy. This process is critical in understanding the limitations and strengths of each algorithm, guiding selection of the most suitable ML and DL algorithm for future optimizations of the μ-PMAM process.

The predicted values of deposition height and deposition width were then compared with their corresponding values in Tables 3.3 and 3.4. This comparison enables evaluation of prediction accuracy of an ML or DL algorithm and how well it could replicate the observed deposition geometry under various process parametric combinations. Such evaluation helps to assess the performance of ML or DL algorithms and identify the areas where the algorithms are either overfitting or underperforming. Performance of the trained, validated, and tested ML and DL algorithms was evaluated in terms of coefficient of determination 'R²' and mean absolute error (MAE) as detailed below. These evaluation criteria provide insights into how well predictions of an ML or DL algorithm align with the corresponding experimental values.

- **Coefficient of Determination *'R²'*:** Value of coefficient of determination *'R²'* indicates closeness of the predicted value of an output parameter with its corresponding experimental value. It provides a measure of the proportion of the variance in a dependent or output parameter predictable from the independent or input parameters. It is computed using Eq. 5.

$$R^2 = 1 - \frac{\sum_{i=1}^{n}(y_i - \hat{y}_i)^2}{\sum_{i=1}^{n}(y_i - \bar{y})^2} \tag{5}$$

  where, $'y_i'$ and $'\widehat{y}_i'$ are the experimental and predicted values of an output parameter respectively for the i^{th} data point; $'\bar{y}'$ is the mean of all the experimental values of that output parameter; and *'n'* is the number of data points. Higher value of *'R²'* is preferable. Its value close to 1 indicates that an ML or DL algorithm is able to capture most of the variance in the data whereas its value close to 0 indicates its poor predictive accuracy.

- **Mean Absolute Error (MAE):** The MAE measures the average magnitude of the errors between predicted and experimental values of all the output parameters. It calculates the average of the absolute differences between predicted values and experimental values

of an output parameter providing a measure of predictive accuracy of an ML and DL algorithm for that parameter. Value of MAE is computed by the Eq. (6).

$$MAE = \frac{1}{n}\sum_{i=1}^{n} | y_i - \hat{y}_i | \quad (6)$$

MAE values of all the output parameters are combined to get overall MAE value of an ML/DL algorithm for its training phase and similarly for its testing phase. A smaller value of overall MAE is preferred because it indicates better predictive performance of an ML or DL algorithm i.e., closeness of the predicted values to the experimental values.

3.8 Selection of Appropriate ML and DL Algorithm

Fig. 3.3 shows comparion of performance of six ML algorihms (Fig. 3.3a) and three DL algorithms (Fig. 3.3b) in terms of computed values of their overall MAE and R^2. Based upon the computed values of *'R^2'* and MAE for the six ML algorithms and three DL algorithms as shown in Fig. 3, (i) RF algorithm was selected for predicting geometry of single-layer depositions because its *'R^2'* value is maximum for both deposition height and width (i.e., 0.96 and 0.98 respectively), and its overall MAE values during training and testing are minimum among all the six ML algorithms. These results suggest that the RF algorithm was able to generalize well to various deposition scenarios, making it the ideal choice for predicting the geometry of single-layer depositions, and (ii) SA-TCN algorithm was selected for predicting geometry of multi-layer depositions because its *'R^2'* value was highest (i.e., 0.977), and MAE value is the lowest (i.e., 0.08) among all the three DL algorithm. It reflects its superior performance in handling the time-series or temporal data, capturing the complicated dependencies between different deposition layers, and in integrating the local and global temporal patterns in the μ-PMAM process.

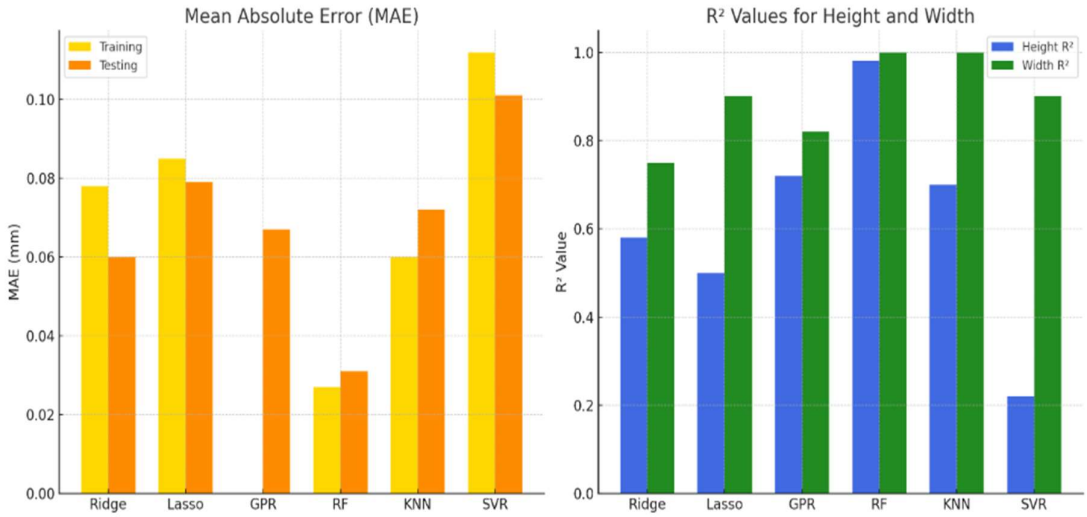

(a)

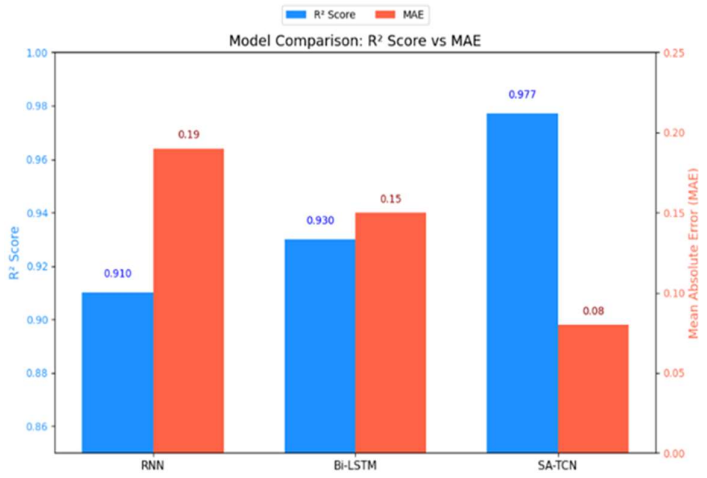

(b)

Fig. 3.3: Performance measures for the (a) six ML algorithms; and (b) three DL algorithms, used in the present study.

3.9 Training of the Selected ML and DL Algorithm

3.9.1 Random Forest Algorithm for Single-Layer Depositions

The RF algorithm is a supervised learning algorithm that builds multiple decision trees during the training process. Each tree is constructed by randomly selecting subsets of both the data and features ensuring diversity in the individual trees. Prediction of particular output parameter is average of the predictions from all the trees and computed using Eq. (7):

$$\hat{y} = \frac{1}{T}\sum_{t=1}^{T}.\hat{y}_t \tag{7}$$

where, $\hat{y}$ is the predicted value of an output parameter (i.e., deposition height or width in the present case); '$\hat{y}_t$ is the prediction made by the t^{th} tree; and *T'* is the total number of trees. By averaging the predictions of multiple trees, the RF algorithm smooths out errors and makes it less sensitive to fluctuations in the data that could otherwise lead to inaccurate predictions. Such aggregation also helps to reduce variance and minimizes overfitting which are common problems in a decision a tree-based algorithm. The RF algorithm provides valuable information by highlighting which input parameters have the most significant influence on the deposition geometry. This allows identification of key input parameters affecting deposition quality and optimizing them for the better results. The selected RF algorithm was trained using the real-time data of Table 3.3 for single-layer depositions of Ti6Al4V. It was able to learn from a wide range of deposition conditions so as to ensure making accurate predictions under new and unseen conditions. Achieving optimum performance of the RF algorithm requires tuning of its hyperparameters such as number of trees *'T'*, maximum depth of trees, and minimum samples per leaf. These hyperparameters

were optimized during its validation. It helps to prevent overfitting, ensuring that the algorithm generalizes well across various deposition scenarios.

3.9.2 SA-TCN Algorithm for Multi-Layer Depositions

The architecture of SA-TCN consists of convolutional layers that extract local features from the data and a self-attention mechanism that enables it to focus on important time steps, effectively capturing the influence of previously deposited layers on the present deposition layer. This self-attention mechanism is especially crucial for multi-layer depositions, where earlier deposition layers play a significant role in shaping the deposition of subsequent layers. By attending to the most relevant time steps, the SA-TCN algorithm makes more informed predictions about the deposition geometry for each layer. Mathematically, the self-attention mechanism is represented by Eq. (8):

$$Attention = softmax\left(\frac{QK^T}{\sqrt{d_k}}\right)V \tag{8}$$

where, *'Q'* is the query vector; *'K'* is the key vector; *'V'* is the value vector; d_k is the dimensions of the key vector. The attention mechanism computes a weighted sum of the values *'V'* based on the similarity between the query vector *'Q'* and key vector *'K'* allowing the algorithm to focus on the most relevant parts of the input data. The selected SA-TCN algorithm was trained using the real-time data of Table 3.4 for multi-layer depositions of SS 316L by feeding the layer index *'N,* µ-plasma power, deposition head traverse rate, feedstock powder flow rate, SOD, height and width of the previously deposited layer *'PreLH'* and *'PreLW'*, and cumulative height *'CumH'* as the input parameters and the weighted multi-modal values of height and width as output parameters. The weighted multi-modal value of deposition height (or width) was computed as summation of product of primary, secondary, and tertiary modal values and their corresponding percentage of occurrence along the deposition length (shown inside the parenthesis for each height or width value). Use of such multi-modal values of deposition height or width helps in better understanding of deposition geometry across deposition length and enables the SA-TCN algorithm to capture both global trends and local variations in the µ-PMAM process. Use of real-time data for training allowed the SA-TCN algorithm to adapt to real-time deposition conditions, ensuring that it could accurately predict the geometry in a variety of practical scenarios.

3.10 Multi-Objective Optimization using NSGA-II

Non-dominated sorting genetic algorithm II (NSGA-II) is widely used powerful evolutionary algorithm that excels in solving multi-objective optimization problems with conflicting objectives. It provides a Pareto front which contains all the non-dominated

solutions ensuring that no single objective is overly prioritized at the expense of others. NSGA-II was used for multi-objective optimization of μ-PMAM process parameters namely μ-plasma power, deposition head traverse rate, and feedstock powder flow rate. From the real-time training data for single and multi-layer depositions (Tables 3.3 and 3.4), those combinations of deposition height and deposition width which have yielded continuous uniform deposition and have the desired aspect ratio, were used as the objective functions for the NSGA-II. Following NSGA-II parameters were used in the multi-objective optimization: 100 as population size; 200 as number of generations; 0.6 as probability of simulated binary crossover; and polynomial mutation probability as 0.2. These parameters define the behaviour of the NSGA-II algorithm and are crucial for ensuring faster convergence to an optimum solution. The population size and number of generations determine how many potential solutions are evaluated and refined over time, while the total function evaluations represent the total number of objective function calculations during the optimization process. The probability of simulated binary crossover and probability of polynomial mutation control how new solutions are generated and varied during the evolutionary process. They contribute to maintain diversity and effectiveness NSGA-II in search of optimum solutions.

Subsequently, NSGA-II was integrated with the RF and SA-TCN algorithm by feeding them with the NSGA-II optimized μ-PMAM process parameters for single-layer and multi-layer depositions respectively. This integration leverages prediction capabilities of RF and SA-TCN algorithm to predict more accurate objective functions. It will help to efficiently evaluate evolutionary solutions particularly when the deposition process is complicated and time-consuming to simulate directly. The objective function $f(\mathrm{P}_i)$ for i^{th} deposition parameter (i.e., deposition height, deposition width, or aspect ratio) was defined as difference between its desired value and its predicted value by RF or SA-TCN algorithm. It was computed using the Eq. 9 and the overall objective function *f(P)* was computed through summation of $f(\mathrm{P}_i)$ values for deposition height, deposition width, and aspect ratio using Eq. 10. Use of such an objective function help NSGA-II to converge to an optimum solution faster with higher accuracy because it reflects absolute error between the predicted and desired values for each deposition parameter.

$$f(\mathrm{P}_i) = \left| y_{\text{pred},i} - y_{\text{desired},i} \right| \tag{9}$$

$$Minimize\ f(P) = \sum_{i=1}^{i=n} f(\mathrm{P}_i) \tag{10}$$

where, $y_{pred,i}$ and $y_{desired,i}$ are respectively ML/DL predicted value and desired value of the i^{th} deposition parameter. The goal of the NSGA-II is to provide a Paero-front between

prediction error in deposition height and deposition width and to identify that optimum combination of μ-PMAM process parameters which will minimize the objective function defined by Eq. 10 which in turn will minimize the overall discrepancy between the predicted and desired values of the deposition geometry parameters.

This **chapter** presented details of selection of deposition material, base plate material and input parameters, real-time data acquisition through video recordings, extraction of images from each recorded video, feature scaling for single-layer depositions, histogram-based multi-modal data preparation for multi-layer depositions, and selection and training of 6 ML and 3 DL algorithms and their evaluation to select the appropriate ML and DL algorithm. It also described training of the selected ML and DL algorithm, and multi-objective optimization of μ-PMAM process parameters by NSGA-II and then by NSGA-II integrated with RF and SA-TCN algorithms for single-layer and multi-layer depositions respectively. The **next chapter** presents the results for predictions by the selected ML and DL algorithm, optimized process parameters by NSGA-II and by NSGA-II integrated with RF and SA-TCN algorithms for single-layer and multi-layer depositions respectively.

Chapter 4

Results and Discussion

This chapter presents the results for predictions by the selected ML and DL algorithm, optimized process parameters by NSGA-II and by NSGA-II integrated with RF and SA-TCN algorithms for single-layer and multi-layer depositions respectively.

4.1 Performance of the Selected ML and DL Algorithms

This section presents prediction performance of the selected ML and DL algorithm for single-layer deposition of Ti6Al4V and multi-layer deposition of SS 316L respectively. Fig. 4.1 depicts comparison of RF algorithm predicted height (Fig. 4.1a) and width (Fig. 4.1b) for single-layer depositions with their corresponding experimental values for validation and testing data (as presented in Table 3.3). Similarly, Fig. 4.2 shows comparison of SA-TCN algorithm predicted height (Fig. 4.2a) and width (Fig. 4.2b) for different layers of a multi-layer deposition with their corresponding experimental values taken from the video No. 9 (mentioned in Table 3.2).

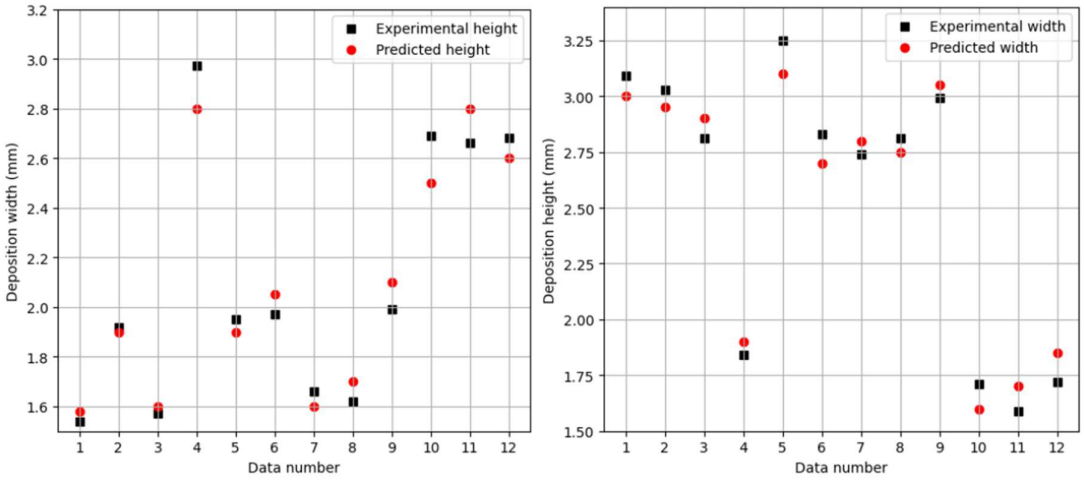

(a) **(b)**

Fig. 4.1: Comparison the RF algorithm predicted single-layer deposition (a) height, and (b) width, with their corresponding experimental values for the validation and testing data.

Graphs of Fig. 4.1 display close agreement the between RF algorithm predicted values of single-layer deposition height and width with their experimental values for all the validation and testing data. This demonstrates high prediction accuracy of the RF algorithm due to its ensemble learning approach, which combines multiple decision trees to minimize overfitting and enhances the generalization. Its robustness to noise and ability to capture non-linear relationships contribute to its precise estimation of single-layer deposition geometry parameters.

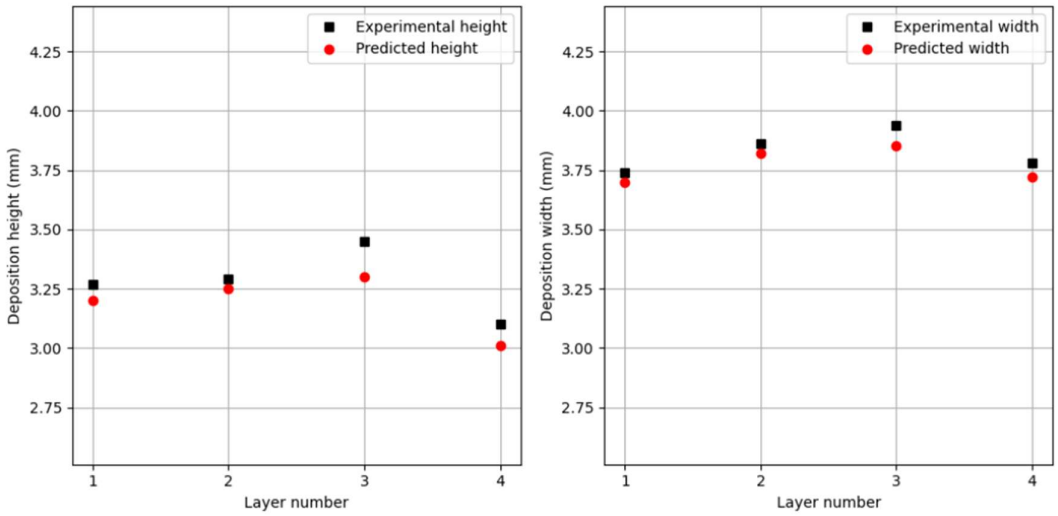

(a) **(b)**

Fig. 4.2: Comparison of the SA-TCN algorithm predicted (a) deposition height, and (b) deposition width for each layer of a multi-layer deposition with their corresponding experimental values taken from their testing data.

Graphs of Fig. 4.2 reveal closeness between SA-TCN predicted values of deposition height and width for all the four layers of a multi-layer deposition corresponding to video no. 9 which is test data in this case. It indicates that the SA-TCN algorithm exhibits very good prediction performance by leveraging both temporal patterns and attention mechanisms. This enables it to capture complex dependencies in the data resulting in highly accurate predictions of deposition height and width.

4.3 Multi-Objective Optimization Results

This section presents results of multi-objective optimization by NSGA-II, and NSGA-II integrated with RF algorithm for the single-layer depositions and NSGA-II integrated with SA-TCN algorithm for the multi-layer depositions.

4.2.1 Results of NSGA-II

Pareto front graphs indicate effectiveness of NSGA-II in multi-objective optimization with the conflicting objectives. Present work focussed on ability of NSGA-II to minimize the prediction error for deposition width and height (i.e., difference between their desired value and NSGA-II optimized value) and its ability to balance the trade-offs between conflicting objectives i.e., deposition height, deposition width. Fig. 4.3a depicts Pareto front graph showing differences between the desired and optimized deposition width on X-axis and differences between the desired and optimized height on Y-axis for single-layer depositions and Fig 4.3b shows the same for the multi-layer depositions.

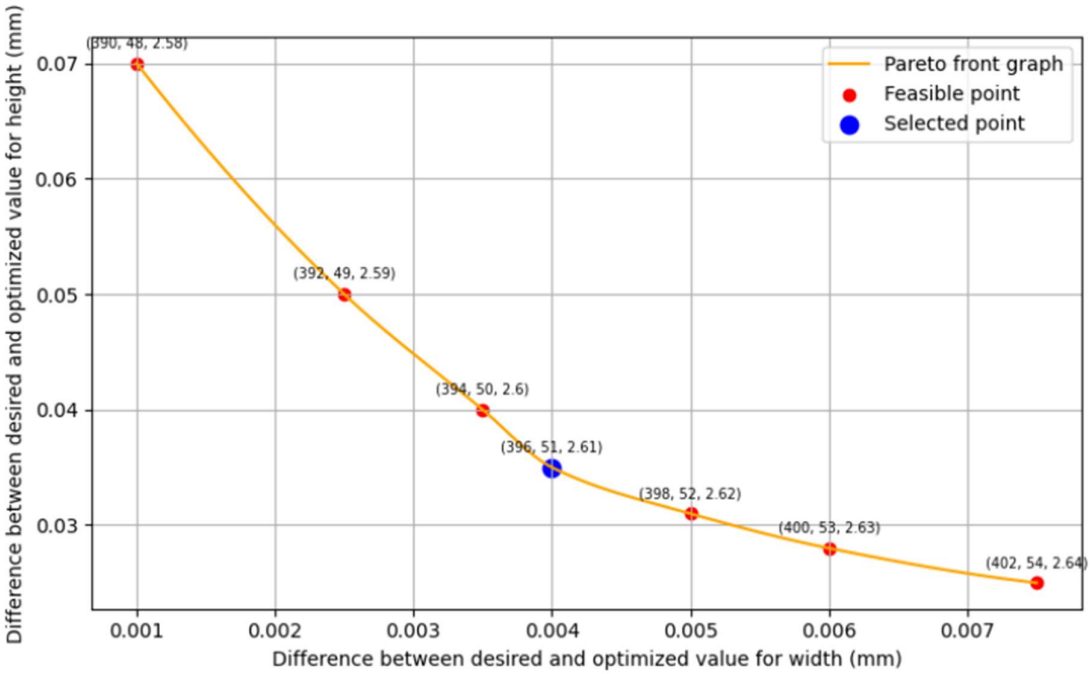

(a)

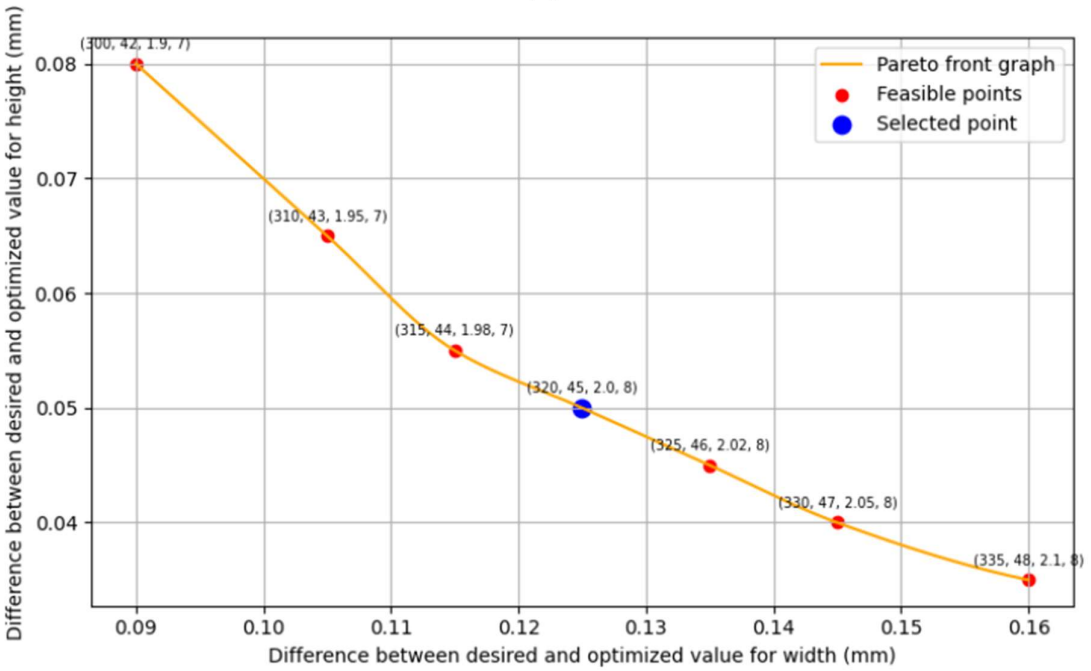

(b)

Fig. 4.3: Pareto fronts for multi-objective optimization by NSGA-II using training data for (a) single-layer depositions, and (b) multi-layer depositions.

The Pareto front graphs of Fig. 4.3 also depict the optimized combination of μ-PMAM process parameters for each plotted feasible point shown in red color and the optimized solution selected by NSGA-II shown in blue color. It can be observed from these Pareto front graphs that (i) decrease in prediction error for deposition width increases prediction error for deposition height and vice-versa for both single and multi-layer depositions. It is

due to the fact that for a given amount of deposition material, deposition width will decrease with increase in deposition height and vice-versa, (ii) the optimized values of μ-plasma power, deposition head traverse rate, and feedstock powder flow rate increase with increase in prediction error for deposition width (or with decrease in prediction error for deposition height), (iii) NSGA-II is able to identify an optimum solution that minimizes the prediction error in both deposition height and width simultaneously through the best trade-off between them. These Pareto front graphs demonstrate effectiveness of NSGA-II in simultaneous optimization of conflicting objectives of deposition width and height.

NSGA-II optimized parameters for single-layer and multi-layer deposition were cross-checked by feeding them to the trained RF and SA-TCN algorithm respectively along with one additional data (taken from real-time training data) which was not used by NSGA-II in the Pareto front graphs of Fig. 4.3. The predicted values of deposition height and width by RF and SA-TCN were used to compute their prediction errors with respect to their desired values. These data are shown in Table 4.1 for single-layer and in Table 4.2 for multi-layer depositions. The predicted values of deposition height and width closely match with their desire values with very low prediction errors. This reflects NSGA-II's strength in handling multi-objective optimization problems where it efficiently balances competing objectives without overly compromising either. This capability is particularly useful in real-time environment of an AM process where consistent and precise control over geometric outcomes directly impacts the structural integrity and surface finish of the fabricated part.

Table 4.1: Percentage error between the desired and the RF predicted geometry parameters for *single-layer* depositions using the NSGA-II optimized process parameters.

Sr. No.	Desired deposition parameters taken real-time training data		NSGA-II optimized process parameters			RF predicted deposition parameters using NSGA-II optimized parameter		Absolute difference between the desired and predicted value (mm)	
	Deposition height (mm)	Deposition width (mm)	μ-plasma power (W)	Deposition head traverse rate (mm/min)	Feedstock powder flow rate (g/min)	Deposition height (mm)	Deposition width (mm)	For deposition height	For deposition width
1	2.13	2.78	396	51	2.6	2.095	2.7760	0.035	0.004
2	2.08	2.73	412	58	2.0	2.0752	2.7305	0.0048	-0.0005

Table 4.2: Percentage error between the desired and the SA-TCN predicted geometry parameters for *multi-layer* depositions using the NSGA-II optimized process parameters.

Sr. No.	Desired deposition parameters taken real-time training data		NSGA-II optimized process parameters				SA-TCN predicted deposition parameters		Absolute difference between the desired and predicted value (mm)	
	Deposition height (mm)	Deposition width (mm)	μ-plasma power (W)	Deposition head traverse rate (mm/min)	Feedstock powder flow rate (g/min)	Stand-off-distance	Deposition height (mm)	Deposition width (mm)	For deposition height	For deposition width
1	3.41	3.87	320	45	2.0	8	3.36	3.745	0.05	0.125
2	3.46	3.95	300	49	2.4	10	3.4427	3.9263	0.0173	0.0237

4.2.2 Results by NSGA-II Integrated with RF Algorithm for Single-Layer Depositions

Table 4.3 presents the optimized process parameters for seven desired combinations of deposition height and width that have yielded continuous and uniform single-layer depositions of Ti6Al4V. The absolute difference between the desired and predicted value of deposition width and height were used as the objective functions in the NSGA-II, and its optimized parameters for each desired combination were fed to the trained RF algorithm to predict their values. The desired and predicted values used to compute prediction error. Only those optimized parameters are presented in Table 4.3 that yielded absolute value of difference between the desired and predicted deposition height and width less than ±0.1 mm thus ensuring best possible match between the predicted and desired deposition geometry. Actual values of the optimized process parameters were rounded-off to get those values of μ-plasma power, deposition head traverse rate, and feedstock powder flow rate which can be set on the CNC machine of μ-PMAM process.

Table 4.3: Optimized process parameters by NSGA-II integrated with the RF algorithm for different combinations of height and width of *single-layer* depositions.

Sr. No.	Desired geometry parameters		NSGA-II optimized process parameters			Absolute difference between the desired and predicted value (mm)	
	Deposition height (mm)	Deposition width (mm)	μ-plasma power (W)	Deposition head traverse rate (mm/min)	Feedstock powder flow rate (g/min)	For deposition height	For deposition width
1.	1.6	2.7	418	62	1.5	0.023	0.033
			420	62	1.7	0.039	0.045
2.	1.7	2.7	420	60	1.7	0.045	0.045
			418	62	1.5	0.021	0.098
			420	65	1.9	0.019	0.055
3.	1.7	2.8	426	62	2.7	0.098	0.092
4.	1.9	3.1	434	60	2.7	0.044	0.023
			438	58	2.5	0.022	0.012
			430	60	2.5	0.067	0.086
			430	52	1.7	0.088	0.094
5.	2.0	3.3	438	52	1.5	0.028	0.022
			438	52	1.9	0.084	0.094
			440	56	2.1	0.097	0.092
			440	56	2.3	0.099	0.077
6.	1.8	3.0	434	56	2.7	0.076	0.098
			438	56	1.5	0.092	0.023
7.	1.8	2.8	426	58	2.5	0.012	0.019
			420	62	1.5	0.091	0.065

It can be observed from Table 4.3 that NSGA-II yielded multiple optimum combinations of μ-PMAM process parameters for some desired combinations of deposition height and width, with each optimum solution meeting the optimization criteria. It highlights its multiple optimum solutions, providing capability due to its evolutionary nature. The result

of this integration was a set of optimized process parameters that maximized the accuracy of the deposition geometry for single-layer deposition of Ti6Al4V. These optimized parameters are critical for achieving uniform layer deposition, controlling dimensional accuracy, and ensuring consistent quality throughout the layer deposition process.

4.2.3 Results of NSGA-II Integrated with SA-TCN Algorithm for Multi-Layer Depositions

Table 4.4 presents the optimized process parameters for the desired combinations of deposition height and width that have yielded four continuous and uniform multi-layer depositions of SS 316L.

Table 4.4: Optimized process parameters by the NSGA-II integrated with the SA-TCN algorithm for different combinations of deposition height and width of *multi-layer* depositions.

Layer No.	Desired geometry parameters		NAGA-II optimized process parameters				Absolute difference between the desired and predicted value (mm)	
	Deposition height (mm)	Deposition width (mm)	SOD (mm)	µ-plasma power (W)	Deposition head traverse rate (mm/min)	Feedstock powder flow rate (g/min)	For deposition height	For deposition width
Deposition # 1								
1	3.61	4.08	8	304	45	2.3	0.12	0.10
2	3.64	4.10					0.19	0.11
3	3.64	4.12					0.20	0.18
4	3.66	4.13					0.19	0.12
5	3.68	4.14					0.14	0.19
6	3.68	4.16					0.09	0.12
Deposition # 2								
1	3.44	3.97	12	290	47	2.8	0.09	0.09
2	3.47	4.01					0.08	0.08
3	3.49	4.05					0.17	0.13
4	3.52	4.10					0.18	0.11
5	3.55	4.14					0.12	0.19
6	3.58	4.19					0.14	0.15
Deposition # 3								
1	3.37	4.03	10	300	46	3.3	0.07	0.18
2	3.39	4.07					0.14	0.11
3	3.40	4.12					0.19	0.14
4	3.40	4.17					0.2	0.09
5	3.42	4.22					0.12	0.11
6	3.43	4.26					0.11	0.19
Deposition # 4								
1	3.66	4.09	8	318	53	3.5	0.09	0.07
2	3.68	4.10					0.11	0.18
3	3.71	4.13					0.18	0.15
4	3.73	4.14					0.12	0.19
5	3.76	4.14					0.16	0.11
6	3.78	4.17					0.12	0.17

The absolute difference between the desired and predicted values of deposition width and height were used as the objective functions in the NSGA-II, and its optimized parameters for each desired combination were fed to train the SA-TCN algorithm to predict their values. The desired and predicted values used to compute prediction error. Only those optimized parameters are presented in Table 4.4 that produced absolute value of difference between the desired and predicted deposition height and width less than ±0.2 mm to ensure the best possible match between the predicted and desired deposition geometry. Actual values of the optimized process parameters were rounded-off to get those values of μ-plasma power, deposition head traverse rate, feedstock powder flow rate and stand-off distance which can be set on the CNC machine of μ-PMAM process. The result of this integration was a set of optimized process parameters that maximized the accuracy of the deposition geometry for multi-layer deposition of SS316L. These optimized parameters are critical for achieving uniform layer deposition, controlling dimensional accuracy, and ensuring consistent quality throughout the multi-layer deposition process.

This **chapter** presented the results for predictions by the selected ML and DL algorithm (i.e., RF and SA-TCN), optimized process parameters by NSGA-II and by NSGA-II integrated with RF and SA-TCN algorithms for single-layer and multi-layer depositions respectively. The **last** chapter summarizes the outcome of the present research in terms of significant achievements, conclusions, and some directions for the future work.

Chapter 5

Conclusions and Scope for Future Work

This chapter presents a summary of the outcome of the present research by presenting its significant achievements, conclusions, and some directions for future works

5.1 Significant Achievements

The work presented in this thesis led to several key achievements in the field of μ-PMAM. The most notable of these are as follows:

- **Development of Optimized Single-Layer Deposition of Ti6Al4V:** The use of ML algorithms, specifically RF, combined with NSGA-II optimization, for the identification of the most effective process parameters for single-layer deposition of Ti6Al4V. This approach successfully minimized the error between the predicted and desired deposition geometries.
- **Multi-Layer Deposition Optimization for SS316L:** By integrating Self-Attention Temporal Convolutional Networks (SA-TCN) with NSGA-II, optimized parameters for multi-layer deposition of SS316L were determined, improving deposition accuracy and part consistency over multiple layers.
- **Enhanced Deposition Geometry Prediction:** The integration of ML and DL algorithms with optimization algorithms allowed for the precise prediction of deposition height, width, and aspect ratio, enhancing both the quality and reproducibility of the parts produced by the μ-PMAM process.

5.2 Conclusions

This research was aimed to predict deposition geometry of single-layer and multi-layer depositions using ML and DL algorithms respectively and multi-objective optimization of μ-PMAM process parameters by NSGA-II integrated with the selection ML and DL algorithm. Following are key conclusions that can be drawn from this study:

- **Accurate Prediction of Deposition Geometry Parameters:** Both the RF and SA-TCN algorithm demonstrated excellent performance in predicting deposition height and width of single-layer and multi-layer depositions respectively.
- **Capturing Inter-layer Interactions:** The SA-TCN algorithm effectively captured the temporal and layer-to-layer dependencies in multi-layer depositions. It offered valuable insights into how previous layers influence the deposition of subsequent layers. This ability to solve for these interactions played a crucial role in optimizing multi-layer depositions.

- **Multi-Objective Optimization of Process Parameters:** Use of NSGA-II integrated with RF and SA-TCN enabled multi-objective optimization of μ-PMAM process parameters (e.g., μ-plasma power, deposition head traverse rate, feedstock powder flow rate) to achieve the desired deposition geometry parameters with minimal error. This led to accurate and consistent results for single-layer and multi-layer deposition of Ti6Al4V and SS316L respectively.
- **Improvements in Part Quality and Consistency:** Using integration of NSGA-II optimized process parameters with predictions by the RF and SA-TCN algorithm represents a significant advancement in optimizing the μ-PMAM process because it ensures that process parameters are fine-tuned to minimize geometry errors and achieve consistent, high-quality deposition. It also reduces need for trial-and-error experimentation thus saving time and resources while ensuring best possible deposition geometry. The optimized parameters not only improve the geometric accuracy of the deposition but also enhance the consistency along the entire deposition length.

5.3 Scope for Future Work

Though the present research has helped significant advancements in optimization of the μ-PMAM process but there lot of scope for the future work on the following aspects:

- **Development of Real-Time Control System:** The integration of real-time process monitoring by computer vision system and feedback loops with ML/DL algorithms could further enhance the optimum performance of μ-PMAM process. It would allow for online adjustment of its process parameters during deposition, leading to even more precise and adaptive manufacturing.
- **Scalability to Complex Geometries:** The current algorithms and optimization strategies could be adapted for predicting and optimizing deposition for more complicated geometries such as multi-axis or overhang structures. This would open new opportunities for creating more intricate and customized parts with enhanced geometrical accuracy.
- **Exploring Additional Materials:** Future research could investigate the application of the methodology of the present work to other materials such as Inconel, Co-Cr-Mo-Ti alloys, and titanium alloys, to assess its generalizability.
- **Wear and Corrosion Testing:** Performance of the optimized deposition geometries could be tested for wear resistance and corrosion behaviour, particularly for applications in aerospace or biomedical devices, where material durability and performance under harsh conditions are critical.

- **Automated Quality Assurance:** The use of AI-based automation systems to conduct post-process quality checks could further reduce manual inspection efforts and improve throughput in production settings. Additionally, automating defect detection and elimination during the deposition process would contribute to higher part consistency and reliability.
- **Development of robust ML/DL Algorithms:** Current ML/DL algorithms are often trained on single-material, single-layer data. Therefore, robust ML/DL algorithms need to developed that generalize across different materials, multi-layer depositions, and more complex geometries.
- **Achieving high dimensional accuracy** directly from CAD models is still a challenge in powder-based AM processes including μ-PMAM process due to process variability and insufficient predictive modelling.

References

Abdulhafedh, A., (2021). Incorporating K-means, Hierarchical Clustering and PCA in Customer Segmentation. ***Journal of City and Development,* 3(1):12-30.** https://www.sciepub.com/jcd/abstract/13053

Baumgartl, L.S., Yan, W., Easton, M.A. (2020). Infrared thermography and deep learning for porosity prediction in LPBF. ***Materials & Design***, 189, 108549. https://doi.org/10.1016/j.matdes.2020.108549

Chandra, P., Singh, R., Gupta, K. (2024). Comparative machine learning models for bead geometry prediction in WAAM. ***The International Journal of Advanced Manufacturing Technology***, 125, 709–723. https://doi.org/10.1007/s00170-023-12045-6

Grill, A., Dietrich, V., Weiler, R. (2019). Scan pattern optimization in LPBF via machine learning. ***AIP Conference Proceedings***, 2042, 020010. https://doi.org/10.1063/1.5082275

Khanzadeh, M., Johnson, L.F., Smith, K.A. (2018). Unsupervised clustering of sensor data for defect detection in laser DED. ***Sensors***, 18(11), 3698. https://doi.org/10.3390/s18113698

Kumar, P., Jain, N.K. (2022). KNN-based surface roughness prediction in micro-plasma transferred arc AM. ***Journal of Materials Research and Technology***, 18, 2106–2117. https://doi.org/10.1016/j.jmrt.2022.03.067

Kwon, S., Park, J., Shin, D. (2020). Closed-loop control of laser DED using deep learning-based defect prediction**. *Journal of Manufacturing Science and Engineering*,** 142(8), 081008. https://doi.org/10.1115/1.4046446

Liu, S., Brice, C., Zhang, X. (2022). Interrelated process-geometry-microstructure relationships for wire-feed laser additive manufacturing. ***Materials Today Communications***, 31, 103794. https://doi.org/10.1016/j.mtcomm.2022.103794

Montazeri, M., Li, L., Verma, R. (2019). Spectroscopic monitoring for anomaly detection in directed energy deposition: A machine learning approach. ***Journal of Materials Processing Technology***, 271, 120–131. https://doi.org/10.1016/j.jmatprotec.2019.03.018

Mukherjee, T., Kar, A., Paul, S. (2020). Machine learning guided WAAM bead stability optimization. ***Journal of Manufacturing Processes***, 54, 541–550. https://doi.org/10.1016/j.jmapro.2020.01.017

Pitis, S., Li, L., Lyle, J., Littman, M. L. (2021). A Validation Tool for Designing Reinforcement Learning Environments. *arXiv preprint* https://arxiv.org/abs/2112.055

Rafiee, M., Farahani, R. D., Therriault, D. (2020). Multi-material 3D and 4D printing: A survey. *Advanced Science*, 7(12), 1902307. https://doi.org/10.1002/advs.201902307

Ren, B., Sun, K., Liu, Q. (2021). Distortion prediction in LPBF using deep learning. ***Materials Today Communications***, 27, 102309. https://doi.org/10.1016/j.mtcomm.2021.102309

Scime, L., Beuth, J. (2018). Automated anomaly detection during powder bed fusion using optical melt pool monitoring. ***Additive Manufacturing***, 21, 503–510. https://doi.org/10.1016/j.addma.2018.05.020

Subadra, S., Patel, M., Rao, P. (2024). Inverse modeling for WAAM process parameters using K-nearest neighbours classification. ***Journal of Manufacturing Processes***, 74, 101–110. https://doi.org/10.1016/j.jmapro.2023.12.011

Tang, Y., Wong, C., Shi, Y. (2020). Deep learning for weld bead defect classification in WAAM. *Welding Journal*, 99(12), 325–334. https://doi.org/10.2351/1.5096245

Wang, H., Chen, L., Zhao, J. (2023). Real-time anomaly detection in LPBF with vision-based deep neural networks. ***Additive Manufacturing***, 66, 102950. https://doi.org/10.1016/j.addma.2023.102950

Xiong, J., Zhang, G., Hu, J. (2019). Artificial neural network for prediction of bead geometry in laser DED. ***Rapid Prototyping Journal***, 25(6), 893–902. https://doi.org/10.1108/RPJ-03-2018-0071

Yuan, P., Song, B., Liang, X. (2018). In-situ defect detection in powder bed fusion using high-resolution imaging and neural networks. ***Journal of Manufacturing Processes***, 35, 623–631. https://doi.org/10.1016/j.jmapro.2018.07.021

Zhang, J., Liu, S., Zhao, Y. (2023). YOLO-based X-ray detection of porosity in WAAM. ***Journal of Nondestructive Evaluation***, 42, 57. https://doi.org/10.1007/s10921-023-00916-5

Zhang, X., Yin, M., Zhao, L. (2021). Vision-based control of bead geometry in laser DED. ***Optics & Laser Technology***, 139, 106874. https://doi.org/10.1016/j.optlastec.2021.106874

Zhang, X., Zhang, Y. (2023). Deep learning: systematic review, models, challenges, and research directions. ***Neural Computing and Applications***, 35(9), 23103–23124. https://doi.org/10.1007/s00521-023-08957-4